MIT Open Access Articles

A brief history of negative triangularity tokamak plasmas

Version: Author's final manuscript: final author's manuscript post peer review, without publisher's formatting or copy editing

Massachusetts Institute of Technology

A brief history of negative triangularity tokamak plasmas

A brief history of negative triangularity tokamak plasmas

A. Marinoni · **O. Sauter** · **S. Coda**

Abstract This review is devoted to tokamak plasmas with a cross sectional shape featuring negative triangularity, which appear to hold great promise as a candidate reactor configuration owing to their improved confinement. A brief historical perspective of its role in the worldwide magnetic fusion program is offered before reviewing theoretical predictions and experimental results on both magneto-hydrodynamic stability and turbulent transport. The material covers more prominently the confined plasma region, while limited work in the published literature is devoted to the scrape-off layer and plasma-wall interactions. A discussion on the suitability of this plasma shape in future reactors concludes the paper.

A. Marinoni
Massachusetts Institute of Technology
Plasma Science and Fusion Center
77 Massachusetts Avenue, NW17, Cambridge (MA) USA
E-mail: marinoni@mit.edu

O. Sauter
Ecole Polytechnique Fédérale de Lausanne (EPFL)
Swiss Plasma Center (SPC)
CH-1015 Lausanne, Switzerland
E-mail: olivier.sauter@epfl.ch

S. Coda
Ecole Polytechnique Fédérale de Lausanne (EPFL)
Swiss Plasma Center (SPC)
CH-1015 Lausanne, Switzerland
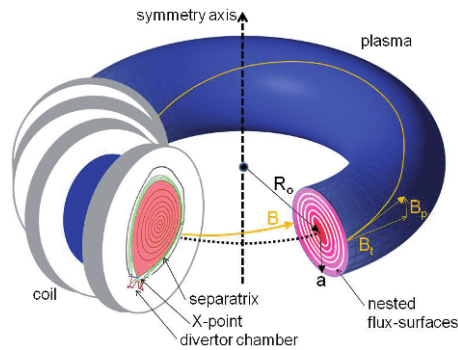E-mail: stefano.coda@epfl.ch

Fig. 1 Cartoon illustrating the equilibrium of a plasma in a tokamak configuration. The toroidal and poloidal components of the confining magnetic field are denoted as B_t and B_p, respectively, while the magnetic axis is represented by a dashed line. For illustration purposes, external coils are reduced to four toroidal field coils.

1 Introduction

The Tokamak is presently the leading candidate for an economically viable magnetically confined nuclear fusion reactor. Tokamaks, conceptualized in the 1950s by Soviet physicists I. Tamm and A. Sakharov [1], make use of an intense magnetic field and an electric current to confine plasmas in the shape of a torus. The spatial coordinate around the axis of symmetry of the torus is called *toroidal*, while the plane orthogonal to the toroidal direction is referred to as the *poloidal* plane. The equilibrium, a cartoon of which is displayed in Fig. 1, is composed of nested surfaces over which a number of quantities, viz. pressure and current density, are approximately constant; the innermost surface degenerates into a toroidal line and is referred to as *magnetic axis* [2]. For any given flux surface, the radial distance of its centroid from the axis of symmetry of the device is called *major radius*, while its half-width on the mid-plane is referred to as *minor radius*.

Many of the early tokamaks, starting with the first-ever-built device *T-1*, employed a near-circular poloidal cross section, which was the natural choice one would make when folding the cylindrical plasma employed in linear devices into a torus. The fusion community began exploring non-circular cross sections in the late 1960s to early 1970s with the goal of either increasing the maximum limit to the current density [3,4,5,6] above the Kruskal-Shafranov limit [7], or to find configurations that would allow the confinement time to exceed the Bohm scaling [8]. It is instructive for the reader not familiar with plasma shaping to visualize a number of poloidal cross sections, some of which will be often referred to in the following, in Fig. 2.

The highest quality of confinement steadily achievable in tokamaks is contingent on operation in scenarios free from the most virulent Magneto-Hydro-Dynamic (MHD) instabilities. As noted by H.P. Furth [9], the radial profile of the electron temperature is determined both by turbulence through the heat transport equation and by MHD stability via the shape of the current density radial profile entering Ohm's law. The overall electron heat diffusivity can then be modelled as the sum of the MHD induced macroscopic contribution, χ_{mhd}, and that due to microscopic fluctuations, χ_{turb}, which generally dominates in the outer part of the poloidal cross section. In the late 1970s-early 1980s, while MHD theory matured to a level sufficient to quantitatively estimate the linear stability for given radial profiles of plasma pressure and current density, the theory of turbulent transport was still very preliminary. In particular, the observation that radial temperature profiles tend to fall within a narrow range
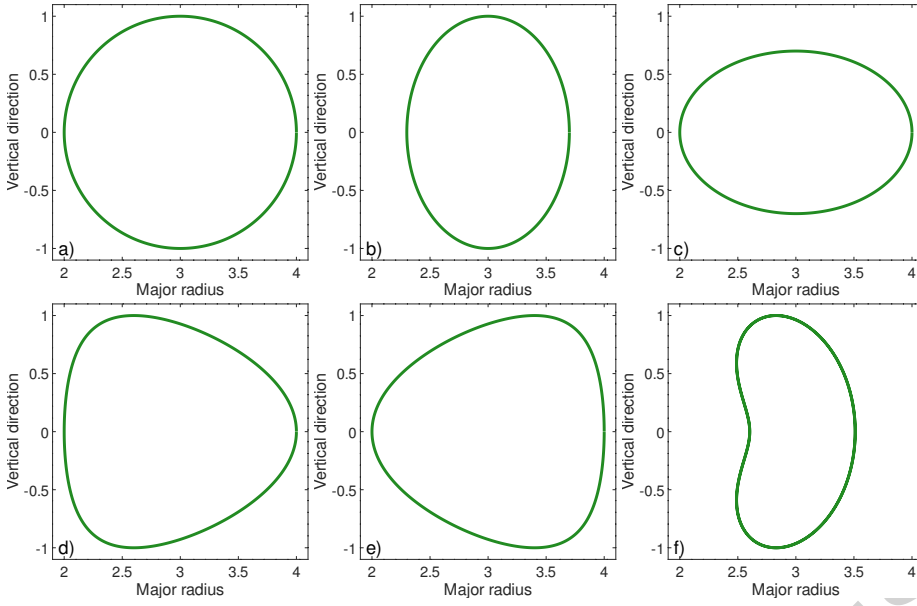
Fig. 2 A few examples of poloidal cross sections used in tokamaks, in arbitrary units, with the axis of symmetry of the torus on the left of each figure. (a) circular, (b) elongated, (c) oblated, (d) *dee* or positive triangularity, (e) *reverse-dee* or negative triangularity, (f) bean.

due to the onset of strong turbulence driven transport beyond a given threshold had just been formulated as the *Principle of Profile Consistency* [10], nowadays known as plasma stiffness, but no quantitative prediction could be made at that time.

It has to be noted that, even to this day, it is generally harder to predict anomalous transport than MHD stability due to the significantly larger computational resources needed. It was apparent, therefore, that a viable way to improve the overall plasma confinement was to minimize the core diffusivity via an optimization of the MHD configuration; additional improvements could be obtained if one was able to reduce turbulence near the plasma edge, thereby creating an insulating layer. The basic idea that guided the MHD optimization principle was to deform the poloidal cross section in a way as to allow one to increase the pressure content of a given plasma while maintaining MHD-quiescent operation. In particular, it was discovered that ballooning modes, a localized pressure driven instability, can be stabilized at higher pressure than that at which they first become unstable [11,12,13]: a phenomenon known as second stability. This resulted in the adoption of *dee-shaped* cross sections, also commonly referred to as *positive triangularity* (PT) shape; *bean-shaped* configurations [14] were also considered (positive triangularity+indentation to provide 2nd ballooning stability conditions) before being later abandoned as their confinement properties proved to be inferior to those of dee shaped plasmas. Cross sectional shapes characterized by a *reversed-dee* configuration, also known as *negative triangularity* (NT), were examined and quickly dismissed on grounds of poor MHD stability.[1] Plasmas at positive triangularity were also attractive on technological grounds because, according to the *Princeton D-coil* design [15], toroidal field (TF) coils are subject to pure tension from $J \wedge B$ forces when they are shaped as a *dee*: the coil is essentially the analogous to the catenary formed by a

---

[1] A number of early papers referred to this configuration as *inverse-dee* or *inverse-triangularity*

hanging chain for currents in a magnetic field whose strenght is inversely proportional to the distance from the axis of symmetry of the torus.[2] The ability of the dee shape to sustain a stable plasma to higher performance was reported by numerous devices worldwide [17, 18, 19, 20] thus providing overwhelmingly convincing validation of the MHD theory. The discovery of the H-mode in the early 1980s [21] provided a robust way of creating the edge insulating layer dubbed Edge Transport Barrier (ETB), where turbulence is stabilized by flow-shear [22, 23], thereby paving the way to the achievement of the conditions necessary for self-sustained nuclear fusion.

In H-mode plasmas the confinement level is strongly correlated to the height of the edge pedestal which, as successfully explained by the theory of peeling-ballooning modes [24], increases with positive triangularity. Although it is beneficial to maximize the core confinement to reduce the capital cost of a power plant for a given power output, other constraints apply. More specifically, the main operational challenge intrinsic to the H-mode regime is that the power flow crossing the plasma edge must remain above the L→H power threshold for the high confinement state to persist. However, parameters in future reactors are such that the power density that will be convected to the vessel will travel along a very narrow channel and will thus be much too large for Plasma Facing Components (PFC) to withstand. Therefore, intense research is being conducted worldwide to obtain stable H-mode regimes in which most of the power is radiated by impurities seeded near the plasma edge, thereby shielding PFCs in a configuration called *detachment* [25], in which a large fraction of the power crossing the plasma edge is radiated by seeded impurities [26]. This strategy is, however, complicated by the fact that impurities are advected inside the plasma through the main ion density gradient in the pedestal, thereby affecting its stability. The L→H power threshold, therefore, gives rise to conflicting requirements dictated by the core and the edge of the plasma, which has recently resulted in a new line of research known as *core-edge integration*. In addition, detached regimes may not be easily controlled experimentally as their operating point is a sensitive function of parameters giving rise to transitions between attached and partially detached conditions known as *detachment cliff* [27]. It has been recently predicted that the detachment cliff is made more severe by steepening radial gradients near the separatrix, due to enhanced poloidally driven plasma flows, which typically happen in the H-mode regime [28]. As a consequence, if reactors were to be maintained in a detached state, it would be easier to control the plasma if it was operated in the L-mode regime, as opposed to H-mode, provided that the global confinement was sufficient to sustain the desired pressure level.

Pedestals, due to their low turbulent levels, also give rise to other issues hampering the H-mode regime. The extremely low transport coefficients characterizing ETBs are such that, at fixed values of energy and particle fluxes, pedestals develop radial pressure gradients large enough to trigger bursting instabilities known as Edge Localized Modes (ELMs). Large and uncontrolled ELMs cannot be tolerated in future reactors because, in the absence of a large expansion of the heat flux footprint on the wall, the energy and particle fluxes they convect to the wall are projected to significantly decrease the lifetime of PFCs [29]. Therefore, unless stable ELM-free H-modes are found, if reactors are to operate in the standard H-mode regimes ELMs will have to be suppressed or mitigated by *active techniques* such as Resonant Magnetic Perturbations (RMPs) or ELM pacing via pellets or periodic vertical movement of the plasma column [30]; whereas, for obvious safety reasons, the use of passive techniques would be much preferred in reactors. Finally, the high particle confinement that

---

[2] When considering stresses out of the plane of the coil, the *Princeton D-coil* shape is no longer an optimal solution [16]

characterizes the H-mode regime causes significant impurity retention, thereby lowering fusion performance due to excessive dilution of the main ion species.

All these issues have recently been made part of the fusion community question whether the H-mode regime is the optimal or, in the worst case scenario, even a viable candidate for operation in future fusion reactors, although it is commonly agreed that H-mode levels of confinement are necessary for a viable DEMO reactor. As a result, alternative magnetic configurations are being explored , or revisited, to look for optimal solutions using the more advanced numerical tools that are now available.One of the most prominent of such alternative configurations is the Negative Triangularity which, as will be explained in Sec. 3, modifies the poloidal cross sectional shape from standard to *reversed-dee* in an effort to improve confinement by reducing χ_{turb} rather than χ_{mhd}.

This paper reviews past and recent experimental and theoretical work on plasmas with a Negative Triangularity shape: the MHD stability properties of this configuration are discussed in Sec. 2 while transport properties are the subject of Sec. 3; fast-ion and exhaust physics aspects are reviewed in Sec. 4 and Sec. 5, respectively, conclusions and future perspectives are offered at the end.

2 Magneto-hydro-dynamic stability

Most of the negative triangularity stability analyses performed until recently relate to the predictions of ideal MHD, which will be the focus of this Section. Ideal MHD is relevant to predicting the overall operational limit in terms of vertical stability for control and in terms of local and global modes for β-limits, i.e. the largest pressure the plasma can stably sustain for a given confining magnetic field. The paper by Medvedev [31] is actually an excellent review of the expected ideal limits of a negative triangularity tokamak and we shall follow in large part this work for the recent results.

We first postulate an equilibrium with the plasma boundary typically defined as follows when designing new tokamaks [32,33]:

$$R(r,\theta) = R_0(r) + r\cos\{\theta + \delta(r)\sin(\theta) - \lambda(r)\sin(2\theta)\}$$
$$Z(r,\theta) = Z_0(r) + \kappa(r)r\sin(\theta), \tag{1}$$

where (R_0, Z_0) are the coordinates of the centroid of the surface, r is the half-width of the surface at the elevation of the centroid and θ is the angle around the poloidal direction, while κ, δ and λ are shaping coefficients that describe the elongation, triangularity and squareness of the surface, respectively; higher order shaping coefficients can be used to further generalize the description. Other types of representations, such as Fourier expansion in the poloidal angle, are sometimes used depending on the application considered. From the usual definition of triangularity [33], δ should be replaced by arcsin[δ] in Eq.1 as is performed in Miller's equilibrium [34], however this leads to less than 10% differences for the typical values $|\delta| < 0.6$ used so far in experiments: the simplification $\arcsin(\delta) \simeq \delta$ will thus be adopted. A first question regarding a target equilibrium is the engineering difficulty and complexity of the toroidal-field and shaping coils. The design of a DEMO negative triangularity tokamak (NTT) has been actively pursued in recent years, thanks to the work of [35, 36,37,38]. A positive triangularity (PT) naturally leads to TF coils with a curved outer shape which is best to reduce stresses. On the other hand, negative triangularity (NT) requires an over-sized design or a long straight TF portion at the LFS, hence potentially increased local curvature at the top/bottom LFS corners and reduced life cycle. This is in part why the early NTT designs used a large number of TF coils [35], however ongoing developments indicate

that this may not be required. The remainder of this section describes the stability properties of axysimmetric ($n = 0$) and non-axysimmetric ($n > 0$) toroidal mode numbers in plasmas at $\delta < 0$ and how they generally compare to more familiar configurations at $\delta > 0$.

2.1 The $n = 0$ ideal stability

The next question relates to the control of such NT plasmas and in particular to the vertical growth rate of the ideal $n = 0$ mode, with and without wall stabilization. It has been shown [31] that a DEMO sized NTT can have $n = 0$ growth rates in a range that can be controlled with modern feedback control systems. However [31] also showed that NT plasmas have typically higher growth rates than PT and that a double-null up-down symmetric DEMO-NT has even higher growth rates. Vertical stability was first analyzed using a rigid displacement model, before full numerical codes were developed at the end of the 70's-beginning of 80's. Around the same time, non-circular shape tokamak plasmas were studied including positive and negative triangularity, also called "triangularization" or normal/standard and reversed/inverse-dee (D) shapes. For example the original work of Rebhan [39,40,41,42], computing rigid displacement stability, analyzed elliptic and triangular Solovev-type equilibria [43] ($p' = cst$ and $TT' = cst$). Rebhan scanned the parameter Q of the Solovev equilibria which essentially determines the triangular deformation leading to elliptical shapes for $Q \approx 0.5$ (for aspect ratio $A = R_0/a = 3$), PT for $Q \approx 0$ or smaller and NT for $Q > 1$. This work also showed that elongation is the main limiting factor, through vertical displacements, for the stability of axisymmetric equilibria and first found that "small aspect ratio and strong triangular deformation (both positive and negative) are favourable" [39], assuming rigid vertical displacements.

A subsequent work [41] found that "slip" modes ($m = 1, n = 0$) were destabilized by triangularity and that feedback control was necessary [42]. The study was extended in [44], using the ERATO code [45], and in [46], using AXISYM. and it was shown that triangularity is destabilizing for $n = 0$ modes (Fig. 2 of [44] and Fig. 3 of [46]) when considering general $n = 0$ deformations. This was also found in [47] using the PEST code [48]. PEST calculations were also shown to compare well with experimental results of the Tokapole II experiments, with an increased $n = 0$ growth rate with increasing $|\delta - 0.1|$ [49].

The first experimental results on NT plasmas had shown that reverse-dee shapes are more unstable than "square" ($\delta = 0$) shapes [50]. Later, experimental results in PDX showed that NT $n = 0$ growth rates were much larger (about three times) than for PT, but could be feedback controlled, confirming also the role of the magnetic decay n-index [51]. The difference between the rigid displacement model and full ideal MHD is particularly true for $Q < 0$ and $Q > 0.8$, that is strong PT or NT, including when a conducting wall is considered [44].

This also shows that present studies of NT should be careful when using a rigid displacement model for feedback control design in particular. The eigenfunction approach also explains well the differences between plasma shapes [44]. Elliptical plasmas feature an essentially vertical displacement ($n = 0$), PT have a maximum amplitude along the HFS straight side while NT plasmas tend to move preferentially towards the strong curvature of the plasma surface, towards the X-point(s). This may explain in part why diverted NT plasmas have a larger $n = 0$ growth rate than PT, and why a PT wall can be stabilizing for NT plasmas if the wall can be close to the NT "X-point(s)" (see e.g. early studies like in [52]).

Plasma pressure can also influence vertical stability and it was first shown in [40] that PT was more favourable than NT in this respect. This was extended using NOVA-W [53] in [54,55] were a strong destabilization of NT plasmas with β_p (ratio of the kinetic pressure
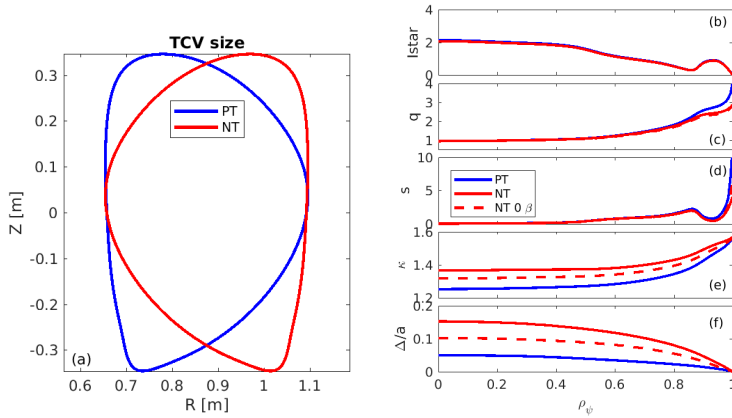
Fig. 3 (a) Example TCV PT and NT shapes, with R flipped around R_{geom}. (b) to (f) using H-mode-like profiles (inspired by PT-H-mode profiles): $Istar = <j_\phi/R> / <1/R>$, q, magnetic shear, elongation and normalized Shafranov shift, $\Delta/a = (R_0(r) - R_0(a))/a$.

to that of the poloidal magnetic field, volume averaged, $\beta_P \equiv 2\mu_0\langle P \rangle_V / \langle B_p^2 \rangle_V$) was found despite the presence of a resistive conformal wall, contrary to PT (Fig. 4 in [55]). This was linked to the Shafranov shift increasing with plasma pressure and squeezing flux surfaces near the LFS nose of PT shapes, effectively reducing elongation in the core. On the contrary, elongation is high in the core of NT plasmas (as shown in Fig. 3(e)) and can increase with β_p, leading to strong destabilization of the $n = 0$ mode [55]. Note that this effect is important for other modes as well and for the magnetic well, as will be discussed below, and also for turbulence transport (Sec. 3).

In the more recent studies, motivated by the more clear confinement improvement observed in TCV L-mode plasmas, as described in Sec. 3, KINX [56] with a resistive wall was used to compare vertical growth rates between top/bottom positive and negative triangularity [57]. It was found that already a $\delta_{top} < 0$ with $\delta_{bottom} > 0$ yields much higher $\gamma_{n=0}$ ($\sim 300\ s^{-1}$ vs $150\ s^{-1}$ for $\delta_{top} > 0$) and even more so with $\delta_{top} < 0$ and $\delta_{bottom} < 0$ ($\gamma_{n=0} \approx 1500\ s^{-1}$). It was also found that $\gamma_{n=0}(NT)$ was very sensitive to the distance to the LFS wall, as well as to holes in the wall due to ports [58]. NT $n = 0$ modes were also shown to be more sensitive to elongation [58]. Optimization can reduce the growth rates to controllable values but in some cases a LFS distance of less than $0.1a - 0.2a$ ($\sim 2 - 5$cm in TCV) is required [31]. For example a double-null with strong $\delta < 0$ was shown to be compatible with the TCV PF-coil limit and to feature a controllable $\gamma_{n=0} \sim 500\ s^{-1}$ with a small LFS gap [59]. In [60], $\delta < 0$ plasmas in RFX-mod2 are considered and compared with PT DEMO-like shapes. They find a similar vertical growth rate, within controllable range of their control system and mainly sensitive to elongation. In this case, similar growth rates are found for single- and double-null. This shows that global trends are recovered and can be reviewed here. However, specifics of the assumed current density profiles and of the machine layout are important for quantitative analyses. Let us also mention another very recent study, using the DINA code [61], [62] that analyzed hot vertical displacement events (VDE) based on HL-2M plasmas. They also find a higher growth rate for $\delta < 0$, with a faster VDE evolution and higher Halo currents in the LFS vacuum vessel, requiring special engineering attention, in particular near the X-point(s) [62].

2.2 The stability of $n > 0$ modes

Once we have equilibria that can be feedback controlled and kept vertically stable, the main operating limits are determined by $n > 0$ ideal modes, and mainly by the global $n = 1$ external kink. We will also discuss internal kink and local modes up to $n = \infty$ ballooning modes [63], in particular related to edge stability limits in H-mode like plasmas. In all of these cases, it was recognized early on that NT plasmas are more unstable because of the absence of a magnetic well (favourable average curvature); which is why PT has been the main line of research for tokamaks from the mid-1980's. However, viable solutions for demonstration fusion power reactors are projected to exist even at $\beta \simeq 3$ [64,65,66] which, as it will be explained in Sec. 3, is a value that has already been achieved in $\delta < 0$ plasmas. As such, the MHD stability of configurations at $\delta < 0$ is deemed to be sufficient for a reactor, although the β limit is still believed to be lower than the maximum value achievable in $\delta > 0$ plasmas.. The magnetic well is important for edge localized modes and the peeling-ballooning stability limit [68]. In [69] analytical equilibria were obtained with a deep magnetic well and high shear with vertically elongated PT as well as with horizontally elongated NT ($\kappa < 1$, comet shape). It was confirmed in [70] that non-circular plasmas have a higher ballooning-β limit with either PT and $\kappa > 1$ or NT and $\kappa < 1$. As discussed in [68] the existence of a magnetic well ($d_M < 0$) can be related to the ideal Mercier term [71]

$$d_M = \tfrac{s^2}{\alpha} D_M, \tag{2}$$

with D_M the ideal Mercier term (criteria: stable if $D_M < 1/4$ or also $-D_I = -D_M + 1/4 > 0$), s the magnetic shear and α the ballooning parameter proportional to the pressure gradient [63]. In this context it is useful to use the dominant triangularity and elongation dependence of D_M [72]. Let us first write the relation obtained by [72] (Eq. (7)) in terms of κ, δ and $\Lambda = d\Delta/dr \approx \beta_p + l_i/2$:

$$D_M = -\tfrac{2rp'}{s^2 B_0^2} \left\{ 1 - q^2 + \tfrac{3q^2}{4} \left[\kappa - 1 + \tfrac{\kappa' r}{2}(1 - 2\Lambda) \right. \right. \\ \left. \left. - \tfrac{(\kappa-1)\delta}{3\varepsilon} \left(5 + \tfrac{\delta' r}{\delta} + \tfrac{\kappa' r}{4(\kappa-1)}(9 - 3\tfrac{\delta' r}{\delta})\right) \right] \right\} \tag{3}$$

Assuming $\kappa' = 0$ and $(\delta/r)' = 0$ (which allows to write $r\delta' = \delta$), we obtain (without assuming $q = 1$ as in [72]):

$$D_M \approx -\tfrac{2rp'}{s^2 B_0^2} \left\{ 1 - q^2 + \tfrac{3q^2(\kappa-1)}{4}\left(1 - \tfrac{2\delta}{\varepsilon}\right) \right\}, \tag{4}$$

with r an equivalent minor radius and $' = d/dr$. It should be noted that δ/ε is about $2\delta_a$ (cst) up to mid-radius and increases to $4\delta_a$ at the edge, with $\delta_a = \delta(LCFS)$ and for TCV aspect ratio, thus it is not small over the whole radius. Note that early analytical expressions obtained by expanding with respect to elongation and triangularity led to analysis showing favourable dependence on negative triangularity [73]. We see from Eq. 4 that D_M changes sign if triangularity is $\lesssim -0.2$ and $\kappa > 1$ or if $\kappa < 1$.

As will appear within this short review, D_M is related to the stability of the peeling-ballooning modes [68,74], of the local modes in general but also of the $n = 1$ internal kink [72,75] and of the global modes through the link with the magnetic well. This explains why, after the early studies up to $\sim$1980, two main types of plasma shapes were studied: D-shaped PT (most MHD stability research from mid 80ś) and comet-shape NT with $\kappa < 1$ (e.g: [76,70], as well as [77] for "horizontal" stability), directly linked to the main

dependence of D_M, Eq. (4). The work of [78] showed that the form of the pressure profile also plays a role in the Mercier stability, in addition to PT. The overall proportionality of plasma β with plasma current I_p [79,80], yielding the normalized pressure performance $\beta_N = \beta[\%]/(I_p[MA]/a[m]B_0[T])$, led naturally to the focusing on D-shape plasmas with high elongation and high current, and in large part to the design of the TCV tokamak in particular [81,32]. On the other hand, recent studies of DEMO-like NTT plasmas [31] show that $\beta_N \sim 3$ can be stable and these values have also been reached experimentally in DIII-D experiments [82,83]. This is related to the difference between the Mercier-Ballooning pressure profile optimization and the limit related to low-n external kink modes. Mercier modes are easily stabilized by non-ideal effects [84], so are not considered for stability boundaries (although D_M influences the stability and global extent of low and high n modes as mentioned above [72,68,31]). The optimized pressure profile obtained with p' near the ballooning limit is usually at significantly higher values than the ones limited by the $n = 1$ external kink. This is why the effective operating boundary is obtained from the $n = 1$ stability limit, see e.g. [32] for the TCV design, especially for PT D-shaped plasmas. The reduced ballooning stability of NT plasmas mainly reduces the difference with the $n = 1$ limit but not necessarily reduce the operating boundary significantly. On the other hand, the absence of a magnetic well influences the access to the 2nd ballooning stability region at low shear, high α which is important for ELM physics [74].

2.2.1 Ballooning modes

The ballooning stability limit ($n = \infty$ modes) [63] and related high n modes have been extensively studied and we shall not attempt to review these results here. We will focus on the studies related to negative triangularity. Present-day tokamak studies focus on the access to the 2nd stability region and its effect on the edge stability of H-mode plasmas with large edge pressure gradient and finite edge current density [74,68]. This access was shown to exist with a sufficiently deep magnetic well (d_M sufficiently negative, $d_M \lesssim -0.6$) [74].

Before reviewing early studies on the effect of shape on ballooning modes, it is instructive to look at the profiles of the ideal Mercier D_M and the magnetic well d_M for two examples, inspired by TCV experiments, with a positive and negative triangularity SND and a current density profile with an edge bootstrap current density and large edge pressure gradients typical of H-modes. The two shapes are shown in Fig. 3(a), with $|\delta| \approx 0.5$ and the LCFS chosen symmetric in R around $R = R_0(LCFS)$. The equilibria have been computed with the CHEASE code [85] with $q_0 = 0.95, \beta_N \approx 1.6$ and the same H-mode like pressure and $I* = < j_\phi/R > / < 1/R >$ profiles. The latter is shown in the top panel of 3(b). The resulting q profiles (c) show the typical difference with $q_{NT} < q_{PT}$ according to the value of triangularity (Eq. (36) [33]). The (average) magnetic shear s (d) is not very different, in particular the dip towards $s \approx 0$ is also present in the NT case. Note a stronger increase in shear near the LCFS for the PT case. We show also the profiles of elongation (e) and Shafranov shift (f) with differences between PT and NT which are typical as mentioned above for the $n = 0$ stability and the role of elongation. Increasing β pushes the flux surfaces to the low field side. With PT, this requires that the flux surfaces be compressed vertically, which explains why the elongation on axis is smaller in PT than in NT, as is the Shafranov shift ($\Delta/a < 5\%$ vs $> 10\%$ in NT). To show that this is a generic feature of NT's, we also plot the profiles obtained with zero pressure in NT (dashed red line). We see that the Shafranov shift is still much larger than the high β PT case. In addition the elongation remains high up to the magnetic axis. As mentioned above, this has an effect on the $n = 0$ growth rate and mode structure. It also increases $D_M \propto \kappa - 1$ and leads to more unstable intermediate n
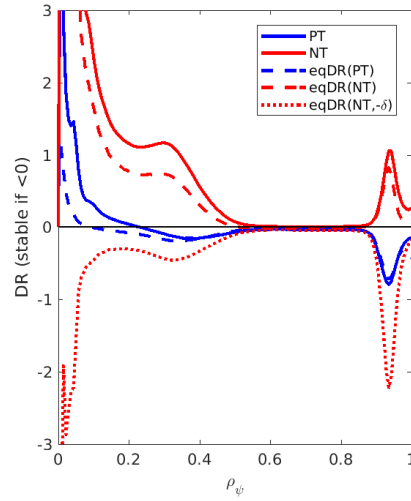
Fig. 4 (a) Mercier term D_M [72], (b) magnetic-well term d_M.

internal modes [31] and $n = 1$ internal kink [72, 75, 86, 87, 88]. On the other hand, increased elongation is favourable for reducing radial turbulent transport and could play a role in the global confinement improvement of NT, as well as the larger Shafranov shift (see Sec. 3).

Using these two equilibria, CHEASE also computes the Mercier term D_M, plotted in Fig. 4 (top panel) along with the magnetic well term d_M (bottom panel). It clearly shows that $D_M(PT) < D_M(NT)$ everywhere, yielding the wide unstable core region with $D_M > 1/4$ related to the destabilization of the internal kink (see below). We also clearly see the opposite peak near $\rho_\psi \sim 0.9$ in the dip of the magnetic shear. D_M is positive, destabilizing, in NT and negative, stabilizing, in PT. This leads to an overall positive d_M, unfavourable average curvature, for NT and the presence of a magnetic well reaching the "deep well" values $d_M < -0.6$ at the edge in PT. The simplified analytic formula, Eq. (4), assumes $\kappa' = 0$ and $(\delta/r)' = 0$, which is mainly valid in the core and for internal kink studies, but not near the edge. To check the direct effect of triangularity, we computed the full analytic formula given in Eq. (3) which is shown as dashed lines in Fig. 4(b), which follow well the exact calculations (solid lines, using Eq. 19 of [85]). We also show the result using the NT parameters inside Eq. (3), but reversing the sign of the terms proportional to δ. This is the dotted red line in Fig. 4(b) which uses the same parameters as the red dashed line (NT case) but with $(-\delta)$ instead of (δ) in the analytic formula. We see that it yields a profile very close to $d_M(PT)$, demonstrating that the flip from positive to negative d_M is only due to the sign of δ over the whole radius. Note that the term related to the Shafranov shift in Eq. (3) is not significant because of the factor cancelling the $\kappa - 1$ term leaving only the small contribution from κ'.

The bad curvature on the LFS is not the only drive for ballooning modes. It was shown in [89] that the local shear also plays an important role. A low or negative local shear is stabilizing [90]. This was confirmed in a series of studies [91, 92, 93] where the ballooning stability near the separatrix was calculated analytically in the case of a divertor, or more precisely of a "bulge" on the LCFS with a much stronger local radial curvature as near the X-point of a single-null (SN) diverted shape. In [89] it is shown that the first stability
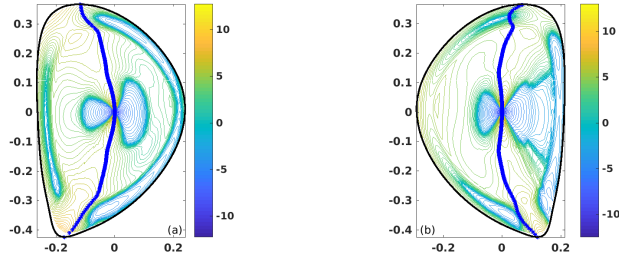
Fig. 5 Separation between good vs bad curvature regions and contours of local magnetic shear in (a) PT (b) NT.

region for ballooning modes is influenced mainly by the length along the flux surface with bad curvature. However the 2nd stability region is obtained if the local shear is small or negative over the whole region of bad curvature. The work in [91,92,93] showed that this can be obtained if the bulge is on the inside (HFS) of the LCFS ($R_{bulge} < R_0$, i.e. θ_{bulge} in the 2nd or 3rd quadrant). However, when the X-point is on the LFS equatorial plane ($\theta_{bulge} = 0$), then the negative local shear cannot extend to the good curvature region and no access to the 2nd stability region is found, even with finite edge current. It was proposed [91, 92,93] that this was the main cause of the difficulty experienced by JT-60 in achieving H-mode [94], since it had such a LFS X-point on the outer mid-plane. These results were confirmed by numerical calculations [95,96] which showed that for $|\theta_{bulge}| < 3\pi/8 \approx 70^o$ there was always a positive local shear region inside the bad curvature region, along the relevant flux surfaces, explaining the lack of 2nd stability access.

In order to demonstrate this important difference between PT and NT, Fig. 5 shows the results from CHEASE of the location of zero curvature (good curvature on the HFS of the blue stars line, bad curvature on the LFS) for the same PT and NT cases shown earlier, as well as the contour of the local shear S. We see that for PT the local maximum of S near the LCFS is in the good curvature region, while it is in the bad curvature region in NT, preventing $S < 0$ over the whole bad curvature region of a given flux surface. Note that this is consistent with the difficulty observed in TCV [97] and DIII-D [98] in entering H-mode in NT plasmas as predicted by [91,92,93]. Fig. 5 explains why the 2nd stability region cannot be obtained in NT. This is also consistent with the pedestal height decreasing significantly as triangularity is decreased [99] and with the H-L transition occurring when the top δ decreases below -0.2 in TCV after the ELMs becoming smaller [100]. Note that -0.2 is also consistent with the value of δ mentioned above below which d_M becomes always positive. This confirms the implications of the results of [99], showing an order of magnitude smaller pedestal height for $\delta < -0.2$ as compared to $\delta > 0.4$ (see Fig. 10 of [99] and Fig. 3 of [35] for a normalized form).

Let us mention that another shape was studied as a result of the quest for 2nd ballooning stability effects. This is the bean shape, which can lead to a fully accessible 2nd stability region with sufficient indentation [101,102,103,104,14] – the opposite case with respect to NT plasmas, for which the access to 2nd stability is closed instead. The bean shape was also shown to be related to extending the negative local shear outside the bad curvature region. The negative local shear at the LFS is due to the local increase of the poloidal magnetic field, itself required to equilibrate the increased pressure gradient when squeezing flux surfaces to the LFS. Using a bean shape, the idea is to squeeze these surfaces even further, increasing B_p in the outer LFS region and changing the local shear further. This was already discussed
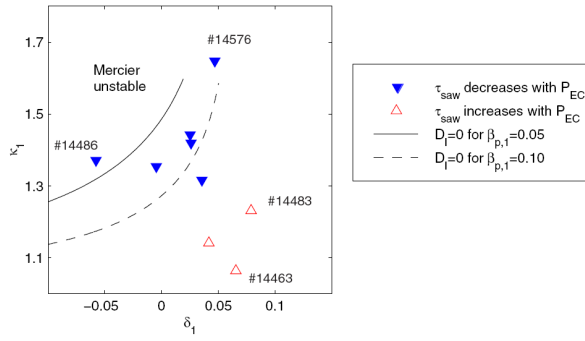
Fig. 6 Sawtooth period response to additional central ECH in terms of elongation and triangularity and related marginal ideal Mercier criteria for two β_p values at $q = 1$ [75].

in [11], when analyzing the local criteria of the 2nd kind. This also showed that the criterion of the first kind (ideal Mercier criterion) is a limiting case of the criterion of the 2nd kind (ballooning mode criterion). Finally, [105] studied the 1st region of ballooning stability, comparing triangularity, bean shape and squareness. This work found that the β_N limit can be compared with the Troyon limit, even with only the 1st stability region, adding a favourable triangularity dependence. It also found that squareness was not favourable.

2.2.2 The $n = 1$ ideal internal kink

TCV experiments demonstrated a striking difference in the behaviour of sawteeth to additional central ECH (electron cyclotron heating) [75, 106, 107, 108]. For small κ and/or large δ, the sawtooth period τ_{saw} increases with ECH power (solid triangles in Fig. 6), while for large κ and/or small/negative δ τ_{saw} decreases with increasing central ECH (open triangles in Fig. 6). We also see that these different behaviors are consistent with the discharges being stable or unstable with respect to the ideal Mercier criterion which depends on both κ and δ as seen in Eq. (4). Another characteristic difference is the fact that the first group (on the stable side of the Mercier term) has peaked pressure profiles in between sawtooth crashes with β_{p1} increasing with ECH power (with $\beta_{p1} = (< p >_1 - p_1)/(B_p^2/2\mu_0)$), while β_{p1} stays small and constant, with flat pressure profiles inside $q = 1$, for the 2nd group in the unstable Mercier zone (Fig. 7 of [75]). This was shown to be consistent with a significant change of the ideal internal kink, using KINX calculations. At small elongation and/or large PT, the ideal internal kink is stable up to $\beta_{p1,crit} > 0.3 - 0.35$ consistent with standard expected values [109]. However for high κ and/or negative δ, the internal kink can be unstable even at $\beta_{p1} = 0$, that is p should remain constant inside $q = 1$ [75, 87, 110]. This confirms the link between the Mercier term and the ideal $n = 1$ internal kink growth rates [72]. This change of behavior is associated with sawteeth being triggered by the ideal trigger condition at low/negative δ instead of the resistive one [111, 112, 87]. Extending these experiments to more negative δ values, the sawtooth period was seen to exhibit a minimum at slightly negative δ, consistent with a maximum in the $n = 1$ ideal growth rate [87, 110]. This non-monotonic behavior was predicted by the derivation of the dominant dependencies of the potential energy of the ideal internal kink with respect to ε, κ and δ [86], which shows terms proportional to δ and δ^2 [86, 87]. The derivation of [86] also shows explicitly that the Mercier term contributes directly to the internal kink δW. Using many KINX simula-

tions, [87] modified the formula used for the ideal kink growth rate to be used for sawtooth modeling (Eq. (16) of [87], for $\varepsilon(LCFS) \sim 1/3$):

$$
\begin{aligned}
\gamma \tau_A &= 0.44 \, \tfrac{\varepsilon_1 \kappa_1}{1 + 7\varepsilon_1 s_1} \, (\beta_{p1} - \beta_{p1}^c), \\
\beta_{p1}^c &= 0.9 - (0.6 + 0.1 s_1) \, \kappa_1,
\end{aligned}
\tag{5}
$$

with the growth rate normalized by the Alfven time τ_A. This shows the significant dependence of $\beta_{p1,crit}$ on elongation and to a lesser extent on shear. An interesting result of these analyses is that the above formula reproduces well the non-monotonic behavior with respect to δ even without an explicit δ dependence in the fit. As discussed in [87] this is due to the different penetration of elongation with triangular shapes. Therefore the κ_1 term in Eq. (5) includes the dependence on δ in a self-consistent equilibrium. It is also noted that the current profile alters $\kappa(\rho)$ as well, which is why s_1 enters in β_{p1}^c, although as a smaller effect. It is important in the case of high elongation, positive δ, which naturally leads to low l_i and where sawteeth are observed to disappear [106,113] and be replaced by a continuous internal mode [113]. The sawteeth were already observed to "disappear" or change behavior at NT, leading then to more unstable q profiles with respect to tearing modes [114]. In [87] it was found that the elongation profile $\kappa(\rho)$ changes again at much stronger negative triangularity, contributing to the overall non-monotonic behavior, i.e. $\kappa(q = 1)/\kappa(edge)$ has a maximum near $\delta \sim 0$ (yielding a maximum ideal n=1 growth rate at slightly NT, see Fig. 17 of [87]). This also shows that full consistent equilibria are required in order to understand these dependencies, even of an internal mode like the n=1 internal kink, which is nevertheless relatively global. A similar change of sawtooth behavior has been observed between bean and elliptical shapes [115].

We shall discuss later the link between MHD and transport, but let us note here the results of [116] which found a similar degradation of the confinement time with respect to ECH power in positive and negative triangularity plasmas. In the same paper, they compare the effect of sweeping the ECH deposition from off-axis to on-axis in a NT and a PT plasma. In this case the confinement is much higher in NT than in PT, but also the relative increase of the scaling factor when heating is deposited inside $q = 1$ is higher for NT. In addition, it shows that the $q = 1$ radius is more central in NT than PT plasmas [116]. Since the $q = 1$ radius can vary when changing the input power, and its radius can be quite central, one has to be careful to not change the relative deposition with respect to the inversion (or near $q = 1$) radius, since it can change significantly the plasma thermal energy and bias the transport studies. The difference in confinement between the low shear region just outside $q = 1$ in NT and PT has not been studied yet.

2.2.3 Resistive modes

Most of the "old" studies were related to the study of the resistive interchange criterion [117], stable if $D_R < 0$ with:

$$
D_R = D_I + (H - \tfrac{1}{2})^2 = D_M + H^2 - H
\tag{6}
$$

Combining the ideal Mercier (Sec. 2.2) and resistive interchange criteria:

$$
D_M - \tfrac{1}{4} < D_R < 0,
\tag{7}
$$

which defines the overall local stability conditions (Ballooning modes have been discussed in Sec. 2.2.1). We see that one needs to be significantly stable to the ideal criterion in order

to be stable to the resistive interchange criterion. The resistive interchange is also a local criterion and, if violated, does not necessarily mean that a finite island [neoclassical] tearing mode ([N]TM) is unstable. However it remains a good indication of the local stability. Therefore, since we have seen that D_M is more unstable for NT plasmas (higher than in PT), D_R is also more unstable. We can look at the triangularity dependence as we did for D_M and d_M in Sec. 2.2 using the same two equilibria, as well as the analytical expansion. Lütjens also derived the main shaping dependencies of D_R in Eq. 5.24 of [118] (transposed here in terms of κ and δ):

$$D_R = D_M(\text{Eq. 3}) - \frac{2rp'}{s^2 B_0^2} s q^2 \left\{ \frac{1}{8} \left(\kappa - 1 + r\kappa' \right) - \Lambda \left[1 - \frac{3}{4} \left(\kappa - 1 + r\kappa' \right) \right] \right. \\ \left. + \frac{\kappa-1}{16} \frac{\delta}{\varepsilon} \left[3 - \frac{r\delta'}{\delta} - \frac{r\kappa'}{\kappa-1} \left(1 + \frac{3r\delta'}{\delta} \right) \right] \right\}. \tag{8}$$

For completeness, if we use the same approximation as for Eq. 4, $\kappa = $ cst and $\delta/r = $ cst, we get (Eq. 5.25 of [118]):

$$D_R = D_M(\text{Eq. 4}) - \frac{2rp'}{s^2 B_0^2} s q^2 \left[\frac{\kappa-1}{8} \left(1 + \frac{\delta}{\varepsilon} \right) - \Lambda \left(1 - \frac{3(\kappa-1)}{4} \right) \right], \tag{9}$$

which yields, including Eq. 4:

$$D_R = -\frac{2rp'}{s^2 B_0^2} s q^2 \left\{ 1 - q^2 + \frac{3q^2(\kappa-1)}{4} \left[1 - \frac{2\delta}{\varepsilon} + \frac{s}{6} \left(1 + \frac{\delta}{\varepsilon} \right) - s\Lambda \left(\frac{4}{3(\kappa-1)} - 1 \right) \right] \right\}. \tag{10}$$

We plot the results using CHEASE of $D_R(\rho)$ in Fig. 7, in the same way as for d_M in Fig. 4. As expected, $D_R(PT)$ is stable while NT is not (in the core and near the edge). It also shows that the analytic expression, Eq. 8, reproduces quite well the exact evaluation (Eq. 20 of [85]). We also show (dotted red line) the result of using the NT equilibrium with Eq. 8 but where the sign in front of the δ only terms have been changed. As in the case of D_M and d_M, the sign of D_R is changed from positive to negative (unstable in NT to stable in PT). In particular the "bump" near the edge, where there is a large pressure gradient and a low shear, changes sign. Thus the absence of a magnetic well also results in an unstable resistive interchange situation. Note that the dotted red line in Fig. 7 over-estimates the equivalent blue dashed line $D_R^{anal}(PT)$, contrary to Fig. 4, bottom panel. This is because the term proportional to Λ (independent of δ) has the $(\kappa-1)/2$ term being cancelled for D_M, Eq. 4, while it adds up for D_R leading to a much larger contribution of the Shafranov shift term: $\Lambda \approx \beta_p + l_i/2$. This also means that NT can become more unstable with increasing β_p, contrary to our standard expectations from PT.

Experimentally, it is not clear yet if there is a fundamental difference between NT and PT for tearing mode stability, or if the latter is indirectly related to the electron temperature profile and whether sawtooth activity can be sustained or not. Early NT experiments already pointed to the appearance of tearing modes when sawteeth disappeared [114]. The only study computing the dependence of the classical tearing mode index Δ' on negative triangularity that we are aware of is in Ref. [119], which shows essentially a quadratic dependence $\Delta' \sim -\delta^2$ (see [120] for more details on the model and the triangularity dependence). Clearly more systematic experimental and theoretical studies on the tearing mode stability in NT are needed.
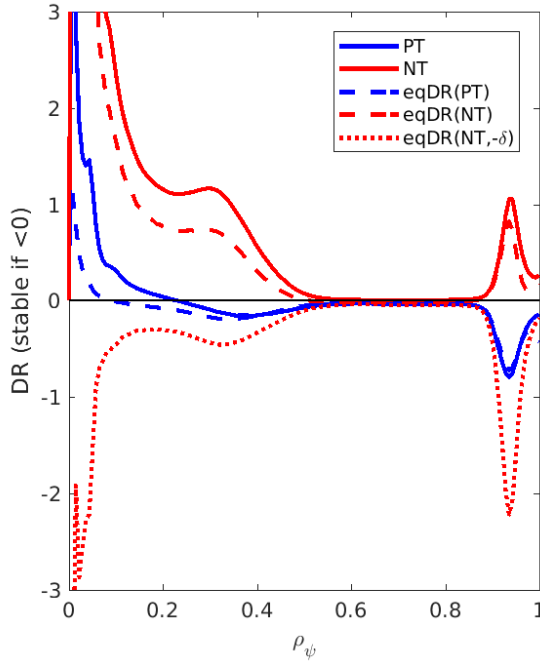
Fig. 7 Resistive interchange parameter D_R and its analytical approximation (Eq. 6 from Eq. 5.24 of [118]).

2.2.4 Global MHD limit

Several theoretical and experimental studies, including triangularity dependence, look at the various aspects of plasma stability, from $n = 0$ to high n, with the aim of determining the global stability boundaries of a given tokamak shape. We shall review them in this Section with the focus on the effective "β"-limit, that is the lowest β-limit determined by ideal MHD $n \geq 1$ modes, and ideal modes which can limit fusion performance. As mentioned earlier this usually means the β-limit defined by the external $n = 1$ kink, where "internal" modes mean modes still unstable with an ideal wall on the plasma surface and "external" modes, those fully stabilized by a wall on the LCFS. Note that internal modes can still have a finite edge displacement for the most unstable eigenfunction, like the $n = 1$ internal kink, but the growth rate is only decreased (typically a factor of two for the internal kink) when a wall is added on the LCFS. Related to these definitions, the "no-wall" stability limit, is the β-limit obtained when the ideal wall is placed very far, practically at more than 10 times the plasma minor radius (in all directions).

Recent experimental results from DIII-D show that $\beta_N \sim 2.7$ can be sustained in NT plasmas [82,83] without tearing activity. Within the power available to the DIII-D experiment, the ideal limit has not been reached. Numerical calculations, carried out with the GATO [121] and DCON[122] codes, based on a DIII-D discharge estimate $\beta_N \sim 3.1$ as the ideal limit without profile optimization [123,83]. As discussed earlier, wall stabilization was predicted to increase the β_N limit by less than 10%, likely due to the L-mode edge yielding small edge currents. DEMO-size NTT also predict ideal limits near or above 3 [31] for in-

ductive type profiles. With reverse shear and bootstrap-aligned current density profile, it is shown in [31] that the magnetic well can be partially recovered, however low shear leads to a lower global low n limit of about $\beta_N \sim 2.1$. Note that PT steady-state plasmas also have a lower β_N-limit than inductive-type monotonic profiles, which is why they rely on wall stabilization. This has not yet been studied in detail for NT shapes. We mentioned the pioneering Asian DEMO-NTT studies described in [35] and refs therein. The EU-DEMO team now also studies NT plasmas, following the conclusion that only a no-ELM regime can be compatible with DEMO requirement [124]. In this respect an L-mode edge NT plasma with a confinement time similar to an equivalent PT H-mode plasma would be ideal. According to predictions by [99] and preliminary experiments on TCV [100], a NT H-mode is characterized by a shallow edge pedestal, resulting in small and frequent ELMs which, in case of transient H-mode transitions, might be tolerated long enough for the control system to safely ramp-down the discharge or return the plasma to the nominal L-mode operation. In addition, as discussed in Sec. 2.2.1, if $min(\delta_{top}, \delta_{bottom}) \lesssim -0.25$ one would not expect H-modes to be triggered. We note that the L→H power threshold may have a triangularity dependence due to fast ions orbit losses, as explained in Sec. 4. The systems-code BLUEPRINT has now been extended to include NT plasmas and will be used for DEMO studies [126]. A preliminary target equilibrium has been generated by the EU-DEMO team, although with a very low q_0 assuming significant fast particle stabilization of the internal kink. This was used to study the internal kink limit, including kinetic effects, in comparison to a PT DEMO plasma [127]. No significant difference in the internal kink stability was found between these NT and PT EU-DEMO plasmas, except a larger growth rate in NT consistent with the earlier results [87, 110]. Sawteeth can lead to significant fast ion transport and reduce fusion performance, therefore these studies are important. Other modes which can reduce fusion power, although not reducing the overall β-limit, are fast ion modes, which will be discussed in Sec. 4.

Regarding ideal stability limit simulations, there is of course too much interesting work to review fairly here. We shall mention a subset with the main bias of looking at triangularity effects. It is interesting to note the blossoming of papers at the 6th international conference on plasma physics and controlled nuclear fusion research in Berchtesgaden in 1976 (published in 1977) studying ideal MHD stability for non-circular plasmas, most of them considering the triangularity dependence down to zero or negative values [128, 129, 130, 131, 132]. This was followed by an interesting workshop in Varenna in 1977 on "finite Beta Theory" [133] and a review paper in [134]. These papers show that equilibria with a wide variety of shapes and β values are possible, but mainly tested their stability against local modes as a first application of the ideal MHD stability codes being developed. Several of these early findings remain valid, such as PT being stabilizing, squareness less favourable and the peakedness of the profiles having significant effects. In the following 2-3 years, the first numerical results on the limit set by the $n = 1$ external kink, including the effects of a conducting wall, were obtained confirming the favourable properties of PT [44, 135, 52] and leading to the studies for JET-shape plasmas [136] (doublets were also studied [46] but are outside the scope of this review). The next major result confirming the advantage of elongation combined with PT to obtain stable high β equilibria was the increasing β-limit with increasing plasma current (up to the $q = 2$ limit) (now known as the Troyon limit [79, 80]).

Apart from the bean shape [103], it is only around the time of the design of TCV that new thorough series of standard PT or racetrack shapes up to very high elongation and high current were studied [32, 137]. This further confirmed the advantage of PT over racetrack and similar studies focusing on high current and high β [138]. Note the new findings during the TCV design phase showing that the stability boundary shrinks and differs from the

Troyon limit at very high elongation ($\kappa \geq 2.5$) [32] (the boundary was later confirmed experimentally in TCV with cases up to $\kappa \sim 2.8$ [139]). These new numerical studies were aiming at using the codes to find the optimum shape, instead of the operating range of a given shape/experiment, albeit solely in regard to the ideal MHD limit. Integrated performance started to be increasingly important with studies for reactor-size tokamaks [140] and the start of the ITER project in March 1987 [141]. As such, the required confinement properties were used as a driver for finding the optimal shape [76]. This leads to a geometry reducing the effects of trapped particle modes thanks to drift reversal and thus to an NT plasma, where most of the trapped particles have their bounce tips in the good curvature region [142, 76], see Sec. 3. This led to a comet shape yielding drift reversal even at zero β [76], when maximizing $J = \int v_\parallel dl$ with plasma shaping [143]. This shape was found stable up to $\beta_N \geq 2$ in [144] which also confirmed the favourable role of NT on trapped particle modes (extended to low aspect ratio as well [145]). Note that this was also associated with lower ITG growth rates in NT plasmas [146], so the 1990's started to have MHD and transport studies integrated to provide a combined physical picture of an "optimum" performance. The transport aspects are detailed in Sec. 3, but we just note here that MHD and transport started to be integrated experimentally in NT plasmas at the same time with the first TCV results showing important differences between NT and PT for both transport and MHD [147, 114].

Regarding ideal global stability boundaries, the main recent results from the last 20 years come from the series of studies conducted by Medvedev et al, first focusing on TCV experimental discharges [57, 58, 59] and then to DEMO-NTT size plasmas [59, 31, 35]. First H-mode like profiles were also considered, but with the goal of an L-mode DEMO-NTT, studies concentrated on L-mode like profiles. The main results are presented in [31] and show stable DEMO-NTT with $\beta_N \geq 3$.

Another important result is the inefficient wall stabilization because of the coupling between internal and external modes, itself related to the lack of magnetic well and to D_M being more unstable in NTs as discussed in Sec. 2.2. This could have an impact for steady-state profiles and resistive wall modes (RWM), since [31] also showed that reverse shear q profiles have a lower limit, $\beta_N \geq 2$, due to the coupling with infernal modes (similar to but possibly more significant than for PT reverse shear q profiles). RWM with advanced scenario q-profiles are of particular interest for steady-state DEMO-NTT studies. At this stage a detailed comparison between NT and PT plasmas with a "standard" monotonic q-profile was performed in [148]. It was also found that the wall-stabilization is less effective for NT than PT, leading to a narrow window for RWMs. Otherwise assuming a wall radius of $1.10a$ for NT and $1.5a$ for a PT DEMO-size case and using MARS-F and MARS-K, [148] found similar behaviour in terms of ideal/resistive wall, plasma flow and drift kinetic effects due to thermal trapped particles. The lack of wall stabilization depends on the effective eigenfunction. In these cases they also find the $n = 1$ ideal kink mode amplitude to be quite localized near the "X-points", similar to the $n = 0$ eigenfunction mentioned earlier and in a similar location as the large positive local shear discussed earlier as well, important for ballooning modes. These effects might be responsible for a stronger coupling observed between local and global modes in NT. Non-linear analyses should provide more insights.

3 Transport

As described in Sec. 2, plasmas with a negative triangularity shape have not received extensive theoretical or experimental attention, at least compared to their standard-dee shaped
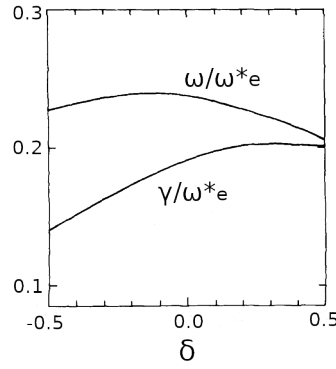
Fig. 8 Mode frequency (ω) and growth-rate (γ), normalized to the electron diamagnetic frequency ($\omega*$), for trapped electron drift modes as a function of triangularity (Reproduced from [142], with the permission of AIP Publishing).

counterparts, on the grounds that they were expected to have poor MHD stability properties. However, as pointed out by T. Okhawa, the transport characteristics of elongated dee-shaped plasmas are, in general, not significantly better than those of circular configurations once the indirect benefit of having a larger toroidal current is factored out. Instead, Okhawa proposed an oblate configuration at negative triangularity in an effort to improve confinement by reducing the fraction of trapped particles that orbit in the bad curvature region [149]. Further analysis work, particularly of MHD stability properties, on such configurations, also termed *comet shapes*, ensued [144]. It is interesting to note that, even before trapped particle instability theories were widely accepted, based only on stability considerations outlined in [4], an oblate shape at negative triangularity was adopted for a detailed design of a power plant edited by R.G. Mills in 1974 [150]. Such design work, however, appeared to have been abandoned in favor of dee-shaped plasmas, which became the prominent configuration in the late 1970s.

3.1 Thermal transport and turbulence

The first work in the realm of transport investigating the effect of $\delta < 0$ can be found in the analysis performed by Rewoldt [142] who, among other classes of instabilities, considered the kinetic linear stability of the trapped-electron drift-wave regime using an electromagnetic code interfaced with a general magneto-hydro-dynamic equilibrium solver. Although the effect of $\delta < 0$ was found to be stabilizing, as shown in Fig. 8, the actual decrease in the growth rate was a factor $3 - 4$ smaller than that due to an increase in elongation, which was therefore deemed to be a more important parameter to focus on in future optimizations.

Negative triangularity configurations were experimentally investigated in the late 1970s on the Poloidal Divertor eXperiment (PDX) tokamak, which was designed to create discharges with a poloidal cross section having standard or elongated dee shapes, as well as with square and reversed-dee configurations. The control system was such that, by progressively varying the radius of the magnetic axis by modifying the vertical magnetic field, plasmas could be moved from one configuration to another continuously. The main design parameters of the PDX tokamak were major radius $R = 1.3 - 1.5$ m, minor radius $a = 0.4$ m, confining magnetic field $B_T = 2.5$ T and plasma current $I_P = 0.5$ MA for a typical pulse

18

length of one second duration. Plasmas were characterized by line averaged density in the range $\langle n_e \rangle = 2 - 4 \cdot 10^{19}$ cm^{-3} and on-axis electron temperature $T_e \leq 1$ keV. All surfaces in contact with the plasma were made from 99% pure titanium. The PDX team reported that the confinement properties of $\delta < 0$ plasmas were quantitatively similar to those measured in more standard configurations, both in ohmic and neutral beam heated discharges [151].

Reversed-dee configurations were also realized in the late 1970s on the Tokapole II tokamak, although research work investigating the impact of triangularity appears to have focused on vertical stability, as discussed in Sec. 2.

3.2 Experiments on the TCV tokamak

After early work in the 1970-1980s, $\delta < 0$ configurations essentially disappeared from the radar of the fusion community until dedicated experiments on the TCV tokamak began in the mid 1990s. The electron energy confinement time of Ohmically heated L-mode plasmas in a wide range of shapes, featuring $1.06 < \kappa < 1.86$, $-0.41 < \delta < 0.72$, was measured to improve with increasing elongation and degrading rather strongly with positive triangularity [152, 114]. However, the fact that the inferred thermal conductivity was found to be rather independent of plasma shaping led to interpreting the observed confinement improvement as mainly due to a variation of the real space electron temperature gradient due to flux surface compression. More specifically, as displayed in Fig. 9 a large fraction of the shape dependence was removed from the confinement time upon normalization to a shape enhancement factor (SEF), defined as the ratio of the confinement time of a shaped plasma to that of the reference cylindrical plasma (see Eq.1 in [152]). This result appears to be consistent with experiments on the PDX tokamak [151] for which confinement was not observed to strongly depend on the sign of triangularity. It has to be noted, however, that the experiments on PDX appear to have been run at moderate values of triangularity and in a somewhat collisional regime, i.e. in conditions for which the stabilizing effect of negative triangularity is not expected to be apparent.
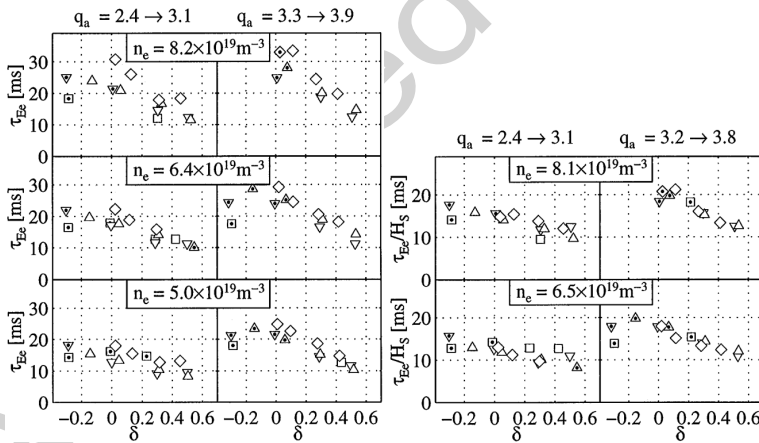

Fig. 9 (Left) Electron energy confinement time as a function of triangularity, sorted by electron density and edge safety factor. (Right) Same data-set with normalization using the shape enhancement factor (Reprinted figure with permission from [152], Copyright by the American Physical Society).

Shortly thereafter, however, Ohmic confinement studies were extended to strong negative triangularity (to $\delta \sim -0.5$) at lower density in MHD-quiescent conditions, and a strong increase in confinement with negative triangularity was observed [153]. This improvement could not be explained by the SEF. At the same time, a refurbishment of the TCV wall allowed the safe utilization of auxiliary heating in $\delta < 0$ discharges, although only in inner-wall limited (IWL) configurations. Subsequent experiments explored the dependence of the electron energy confinement time on plasma shaping in L-mode plasmas with applied centrally deposited electron cyclotron heating (ECH). The effect of plasma shaping was studied by varying the elongation and triangularity of the last closed flux surface (LCFS) in the range $1.1 < \kappa < 2.15$ and $-0.65 < \delta < 0.55$, for values of the engineering safety factor corresponding to 1.7 and 3. The central electron density was maintained below $2.5 \times 10^{19}\,\mathrm{m}^{-3}$, in contrast to the initial ohmically heated experiments previously described, for which the central density was $2-3$ times larger. A clear improvement of confinement with negative triangularity was documented also in these conditions. The overall scaling of the energy confinement time on triangularity was cast in the form [107]

$$\tau_E \propto (1+\delta)^{-0.35 \pm 0.3}, \tag{11}$$

which illustrates the beneficial impact of $\delta < 0$ on the overall confinement.

Based on these early results, the TCV program embarked on a large set of experiments aimed at studying the dependence of confinement on triangularity while disentangling other factors that are predicted to affect the underlying turbulence, such as safety factor, collisionality, electron temperature, density as well as their spatial scale lengths. Experiments were limited to L-mode plasmas because that would make it easier to extract the dependence of core transport on triangularity. Indeed, as in PT H-mode the pedestal height was expected to depend on triangularity, as was later experimentally confirmed [100] and quantified by modeling [99], the direct triangularity dependence of the overall confinement would be entangled with the confinement dependence on the edge pedestal height. More specifically, the dependence of the electron heat diffusivity was probed with respect to the electron temperature and its radial gradient, as well as to density within values compatible with near full EC first pass absorption, by varying the amount of ECH coupled power and its deposition location. The electron heat diffusivity was observed to significantly decrease at negative triangularity, even when normalizing values to a $T^{3/2}$ gyro-Bohm dependence to account for local variations of the electron temperature. Notably, in $\delta > 0$ and $\delta < 0$ plasmas with matched values of elongation and absolute value of triangularity at the LCFS, the same electron density and temperature profiles were obtained when half the EC power was coupled into the latter case, thus demonstrating that $\delta < 0$ L-mode plasmas sustain an H-mode level of confinement [154, 155]. The observed dependence of the mid-radius electron heat diffusivity on the electron temperature, density and effective charge was cast in a unique dependence on the plasma effective collisionality, as displayed in Fig. 10. This was found to be consistent with linear simulations performed with the GLF23 model [156] which indicated trapped electron modes (TEM) as the dominant instability at play in those discharges [157]. Later experiments compared $\delta < 0$ to $\delta > 0$ configurations in terms of the characteristics of turbulent fluctuations measured by the correlation electron cyclotron emission (CECE) and tangential phase contrast imaging (TPCI) [158] diagnostics. In ohmic discharges, the intensity of electron temperature fluctuations is strongly reduced at $\delta < 0$ in the outer half of the plasma volume, while at mid-radius the $\delta < 0$ broadband fluctuation level falls below the instrumental noise floor, precluding a quantitative assessment of the difference between the two cases there. Additionally, a threshold behavior was observed in the outer half of
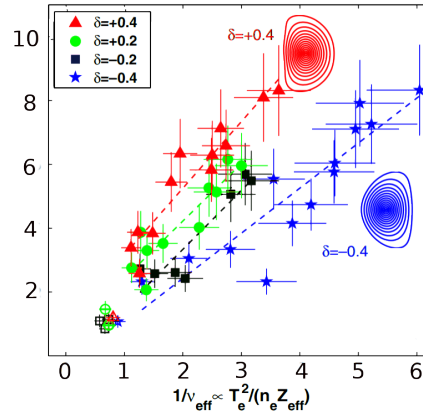
Fig. 10 Mid-radius electron heat diffusivities vs inverse collisionality for a number of EC heated IWL discharges at varying values of triangularity of the LCFS (Reproduced from [157], with the permission of IAEA Publishing)).
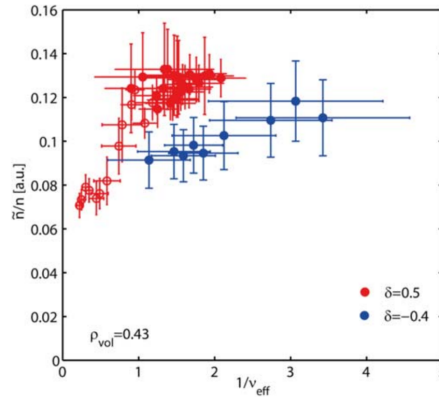

Fig. 11 Relative density fluctuation amplitude as a function of the reciprocal of effective collisionality for plasmas with triangularity values at the LCFS equal to $\delta = 0.5$ (red) and $\delta = -0.4$ (blue), Ohmic (open symbols) and ECH L-mode (full symbols) TCV discharges (ⓒ IOP Publishing. Reproduced with permission from [161]. All rights reserved).

the minor radius only at $\delta > 0$, suggesting that, at least in the ohmic cases considered, the $\delta < 0$ case was characterized by a higher threshold for the onset of the instability [159, 160].

Similar results were obtained when monitoring electron density fluctuations using the TPCI diagnostic in EC heated discharges. More specifically, the absolute intensity of fluctuations was observed to halve at $\delta < 0$ as compared to $\delta > 0$, along with a reduction of the spectral index. As opposed to the ECE measurements in ohmic discharges, the TPCI diagnostic could resolve $\delta < 0$ fluctuations well into the core, and showed that the reduction at $\delta < 0$ extends to mid radius, despite the fact that the local value of δ therein essentially vanishes [161, 162]. The stabilizing effect of the effective collisionality was also observed with TPCI measurements, as displayed in Fig. 11, consistent with results reported in [157, 163].

These investigations of core turbulence were recently complemented by measurements of turbulence in the scrape-off layer (SOL) with both wall-mounted Langmuir probes and a gas puff imaging system. There too, a strong reduction in fluctuation amplitudes is observed for $\delta < -0.25$, accompanied by nearly full suppression of plasma interactions with the first wall [164]. An analysis of different possible correlations and causations points at the shorter connection length in $\delta < 0$ plasmas as possibly the most crucial element behind this phenomenon. It should be noted that a negative-triangularity TCV plasma features among a set of shapes that were used for validation of SOL turbulence simulations by the GBS code by means of reciprocating probe measurements [165]. More recently, thanks to the installation of a neutral beam heating system, the TCV team started exploring the impact of triangularity on confinement in regimes where the ion temperature is close to or higher than that of electrons, thereby complementing earlier results for which $T_i \ll T_e$. Comparison discharges with edge triangularity $\delta = \pm 0.4$ were executed at elongation $\kappa = 1.4$ and line averaged density $\langle n_e \rangle \simeq 2 \times 10^{19} \, \mathrm{m}^{-3}$. It was chosen to approximately match the safety factor between the two plasma shapes, with $q_{95} \simeq 3.4$, thereby increasing the plasma current in the $\delta > 0$ discharge by about 18%; this is a conservative choice when it comes to comparing confinement improvements at $\delta < 0$ because of the positive correlation between stored energy and plasma current which is generally observed in tokamaks. Improved confinement was demonstrated both at fixed auxiliary power, which yielded higher stored energy at $\delta < 0$, and with matched profiles, which required lower coupled power at $\delta < 0$. Consistent with the improved confinement, the intensity of electron temperature fluctuations measured by the CECE system was always observed to decrease at $\delta < 0$ at comparable values of collisionality, electron to ion temperature ratio, and density and temperature inverse scale lengths [166, 160]. With NBI, the highest performances have been achieved on TCV in terms of both β_N and confinement enhancement $H_{98,y2}$, reaching, respectively, 2 and 1.3 with 0.5 MW power, albeit in a non-stationary manner [167]. Among the latest reported developments on TCV is also the establishment of a fully diverted shape in the upper part of the chamber, which, with Ohmic heating, confirms the favorable properties of negative triangularity [167] (Fig. 12). Studies of H-mode $\delta < 0$ plasmas were also conducted in TCV using hybrid diverted shapes with positive lower triangularity and upper triangularity varying from positive to negative [100]. Discharges where heated using EC system with $500 - 700$ kW at the third harmonic (X3) for distributed core heating, and $300 - 900$ kW of second harmonic (X2) for heating localized near the $\rho = 0.9$ surface close to the X-point. The resulting mid-radius collisionality was close to unity which, based on results from [157], is expected to result in a modest stabilizing effect of $\delta < 0$. Correspondingly, global confinement was found to be *reduced* in such scenarios, compared with standard $\delta > 0$ cases, and this could be imputed to the 20% lowered edge pedestal pressure. The lower pedestal height resulted in a concomitant passive mitigation effect on ELMs, as discussed in Sec. 2.

3.3 Theoretical studies

A non-linear gyro-kinetic analysis carried out using the flux-tube GS2 [168] code confirmed that the TCV ECH L-mode discharges were TEM dominated, and quantitatively reproduced the dependence of the core electron heat diffusivity both on triangularity and collisionality [163, 169], as displayed in Fig. 13. However, agreement with experiments within error bars was found only in the outer part of the poloidal cross section, with the predicted stabilizing effect of $\delta < 0$ progressively vanishing towards the magnetic axis. Such result was interpreted to be due to the modest radial penetration length of triangularity (at $\rho = 0.7$ it is
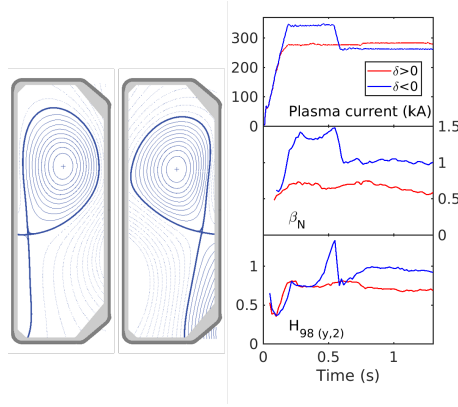
Fig. 12 (Left) Positive- and negative-triangularity diverted TCV plasmas and (right) comparison of plasma current (top), normalized β (middle), and $H_{98,y2}$ confinement-enhancement factor (bottom)
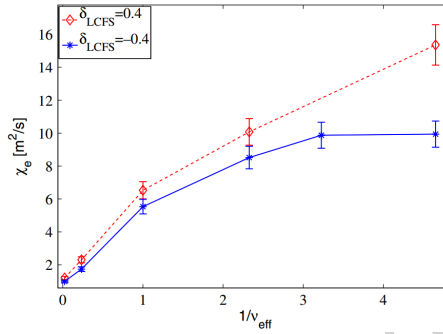

Fig. 13 Predicted electron heat diffusivity as a function of the inverse effective collisionality for $\delta > 0$ TCV discharge #28014 (- -) and $\delta < 0$ counterpart #28008 (-), computed for identical density and temperature profiles of all kinetic species (© IOP Publishing. Reproduced with permission from [163]. All rights reserved).

one-half the value at the boundary), which causes the flux tube simulations to fail to discern significant differences between the two scenarios as the flux surfaces progressively approach the shape of an oval at inner radii. This result suggested that profile shearing effects might be important in determining the overall stability of these discharges [163]. Subsequent studies carried out with the flux tube version of the GENE non-linear gyro-kinetic code [170] confirmed the GS2 results [171,172]. In the GENE simulations, the impact of triangularity on micro-stability was evaluated also near the LCFS, where the largest stabilizing effect of $\delta < 0$ was found, consistent with the largest absolute variation of triangularity. Additionally, by varying the density and temperature scale lengths and taking linear extrapolations with respect to the driving gradient, it was estimated that the critical temperature gradient increases at $\delta < 0$, while no significant impact of the density inverse scale length was found in either equilibrium. The fact that the largest impact of $\delta < 0$ was found, from a gyro-kinetic stand-point, near the LCFS is qualitatively consistent with dedicated experiments, reported in [173], designed to obtain high resolution electron and density profiles by executing repeat discharges at slightly different vertical positions in the vacuum chamber so as to effectively enhance the spatial resolution of the electron pressure profiles measured by the Thomson Scattering diagnostic. While the plasma region within 60-70% of the total volume featured

a rather constant logarithmic temperature gradient for both triangularities, indicating a high degree of profile resiliency, the outer region was characterized by a constant gradient, with the $\delta < 0$ case exhibiting steeper radial profiles for very similar heat flux values.

Further insights into the GS2 modeling revealed that, at fixed density and temperature profiles, the stabilization observed at negative triangularity is due to a combined effect of the perpendicular drifts and of the ballooning eikonal, which reflects the effect of magnetic shear and can be interpreted as the perpendicular wave-vector $k_\perp$. More specifically, the overall stabilization is a result of the modification exerted by triangularity on the toroidal precession drift of trapped electrons. This is intuitively in agreement with the basic desta-bilization mechanism of the collisionless TEM which, as first derived in [174], is given by the resonance between a given wave (e.g. a pressure driven drift wave) and the toroidal pre-cession drift of trapped electrons, with the resulting dispersion relation in a pure plasma being

$$\left(\frac{1}{T_e} + \frac{1}{T_i}\right)\tilde{\phi} = \sqrt{\varepsilon}\left(\frac{1}{T_i}\frac{\omega - \omega_{*,i}}{\omega - \omega_{D,i}} + \frac{1}{T_e}\frac{\omega + \omega_{*,e}}{\omega + \omega_{D,e}}\right)\langle\tilde{\phi}\rangle. \tag{12}$$

In Eq. 12, T_x is the temperature of the generic plasma species x, $\omega_{*,x}$ and $\omega_{D,x}$ are, re-spectively, the diamagnetic drift and the toroidal precession drift angular frequencies, ε the inverse aspect ratio of the machine, $\tilde{\phi}$ the perturbed electrostatic potential, and the an-gular bracket refers to averaging along the bounce trajectory of the trapped particle. In the particular case of perfect equipartition, i.e. $T_e = T_i$, so that $\omega_{*,i} = -\omega_{*,e} \equiv -\omega_*$ and $\omega_{D,i} = -\omega_{D,e} \equiv \omega_D$, Eq. 12 reduces to

$$\omega^2 = \omega_D^2 + \sqrt{\varepsilon}\omega_D\omega_*, \tag{13}$$

from which it is apparent that a necessary condition for the instability to arise is that the toroidal precession drift and the diamagnetic drift have to be oriented in opposite directions. In the limit of a circular plasma at large aspect ratio and low β, the toroidal precession drift of a trapped electron of mass m and velocity v orbiting on a given flux surface ψ can be written as [174]

$$\omega_{D,e} = \frac{m}{2e}\frac{\partial J}{\partial\psi}\bigg/\frac{\partial J}{\partial v^2} \propto G(s, \varkappa)v^2 \tag{14}$$

where J is the second adiabatic invariant, s the magnetic shear, $\varkappa$ a modified pitch angle variable and G is defined as

$$G(s, \varkappa) \equiv \left[2\frac{E(\varkappa)}{K(\varkappa)} - 1\right] + 4s\left[\frac{E(\varkappa)}{K(\varkappa)} - 1 + \varkappa\right], \tag{15}$$

where $E(\varkappa)$ and $K(\varkappa)$ are the complete elliptic integrals of the first and second kind, re-spectively. The shape factor $G(s, \varkappa)$, which is displayed in Fig. 14 as a function of the pitch angle variable $\varkappa$, does not depend on the magnetic shear in the limits of deeply and barely trapped particles, i.e. $\lim_{\varkappa\to 0,1} G(s, \varkappa)$, and is monotonically decreasing across the entire pitch angle space for decreasing values of the magnetic shear. Based on Eq. 13, TEM modes are expected to be weakened or suppressed at negative values of the magnetic shear, a con-dition often associated with reduced turbulence characterizing Internal Transport Barriers (ITB) [175]The physics of ITBs is not the subject of this paper; we note, however, that tur-bulence quenching mechanisms in ITBs have also been widely associated to other factors, of which the most common is increased flow shear. A general analytic expression for the toroidal precession drift in general geometry and finite pressure was derived in [176], in which the impact of elongation and triangularity on the toroidal precession drift were eval-uated for the IWL TCV discharges described above [157]. While triangularity is found to
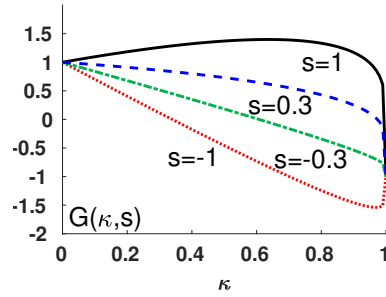
Fig. 14 Pitch angle dependence of the $G(s,\varkappa)$ factor from Eq. 15 for a few values of the magnetic shear s.

have a negligible effect on passing electrons, the impact on trapped electrons is far greater. More specifically, the drift increases at $\delta < 0$ across most of the pitch angle space, whereas deeply trapped electrons drift more slowly when the triangularity is negative. This is consistent with the pitch angle dependence of the non-linear energy flux computed by GS2 and reported in [163] for which, when comparing $\delta < 0$ to $\delta > 0$ equilibria, deeply trapped electrons are on average closer to the resonance condition in Eq. 12, while they are further away everywhere else in the pitch angle space, resulting in a net overall stabilization. It is interesting to note that, consistent with the drift precession predictions [176], also the GS2 non-linear gyrokinetic simulations found a negligible stabilization exerted by negative triangularity on passing electrons [163].

The interpretation based on the modification of the toroidal precession drift is valid locally, meaning that the extent of the induced stabilization depends on the triangularity value of the given flux surface under consideration. Indeed, while the experimental results reported in [157] reconstructed a uniform reduction of the electron heat diffusivity across the plasma cross section, non-linear local gyro-kinetic modeling work [163,171] recovered the experimental results only in the outer part of the cross section, consistent with the local value of triangularity quickly decreasing towards the magnetic axis. While it was immediately realized that such discrepancy hinted at global effects, such impact has only been very recently demonstrated using gradient driven global non-linear gyro-kinetic simulations, which found quantitative agreement across a large fraction of the minor radius between predicted non-linear fluxes and the corresponding experimental values derived from a power balance analysis [177]. In that work it was also concluded that global effects appeared important for the $\delta < 0$ case but not for the $\delta > 0$ case, for which flux-tube simulations yielded adequate results.

The stabilizing effect of $\delta < 0$ is not restricted to TEM dominated turbulence, as evidenced by non-linear gyrokinetic simulations of the more recent TCV discharges which, being NBI heated, are characterized by mixed TEM/ITG [178]. This is consistent with NBI-EC heated DIII-D discharges, reported in Sec. 3.4, and the corresponding gyrokinetic modeling [83]. It is interesting to point out that, even in the case of ITG dominated turbulence that will likely characterize future reactors, the overall transport level is expected to be reduced by decreasing the strength of the sub dominant TEM, as long as their drive is not negligible. The fact that ITG modes are strengthened in the presence of sub dominant TEM turbulence appears to be a rather general property of plasmas in various configurations and has been obtained by a number of authors with both gyro-fluid and gyro-kinetic simulations [179,146]. This may have beneficial consequences for a $\delta < 0$ reactor, for which the

A. Marinoni - O. Sauter - S. Coda

sub dominant TEM are expected to be weakened by the effect exerted by plasma shape, although this effect has yet to be quantified.

3.4 Experiments on the DIII-D tokamak

In 2016 the DIII-D team began a series of experiments aimed at validating the results obtained on TCV. All plasma discharges were carried out, as on TCV, in an IWL configuration because portions of the outer-wall on DIII-D are not armored to withstand the power flux at the strike locations at any power level. Plasmas were designed to be up-down symmetric with the LCFS featuring moderate triangularity $\delta = -0.4$, while coil positioning on DIII-D is such that plasma elongation was fixed at $\kappa = 1.33$. Comparison discharges at $\delta > 0$ were made by developing a mirrored shape with identical elongation but opposite value of triangularity, resulting in the two shapes having the same cross sectional area. In order to establish a link with the TCV results, experiments were first carried out with pure electron heating, resulting in $\delta < 0$ configurations featuring about 30% improved confinement as compared to $\delta > 0$ counterparts at matched values of plasma current, confining magnetic field, line averaged density and auxiliary power. The confinement improvement was significantly lower than that observed in [157], consistent with the fact that, due to the much lower power per particle available in these EC-only heated discharges on DIII-D as compared to those on TCV, plasmas were operated in an intermediate collisionality region, corresponding to $\nu_{eff} \simeq 0.5$ near mid-radius, where the beneficial effect of $\delta < 0$ is marginal [154, 180].

Auxiliary power from the Neutral Beam Injection (NBI) system was subsequently gradually increased, contingent on no sign of overheating of the outer-wall. At the maximum power level allowed, NB heating resulted in discharges sustaining H-mode grade confinement and pressure levels equal to $\beta_N \simeq 3$ and $H_{98,y2} \simeq 1$, respectively, for several energy confinement times, despite relaxed edge pressure profiles typical of an L-mode regime [82, 83]. The persistence of the L-mode regime at auxiliary power levels that far exceed the expected H-mode power threshold is attributed, as explained in Sec. 2, to the stability of ballooning modes [181]. An example of the time evolution of a typical plasma discharge is displayed in Fig. 15, where high confinement is sustained with an L-mode edge as evidenced by the ELM–free D_α signal. The fact that the confinement enhancement factor seen in Fig. 15 improves with increasing auxiliary power is understood in terms of a power degradation of thermal confinement that, although finite, is weaker than that expected from conventional power scaling laws. When the fast ion energy is accounted for, these $\delta < 0$ discharges displayed a near-zero power degradation of total confinement [82, 83]; this is in contrast to the ITER-89P scaling law that features a total stored energy proportional to the squared root of the auxiliary coupled power.

Linear gyro-kinetic and gyro-fluid analysis performed with the CGYRO [182] and TGLF [183] codes, respectively, showed that TEM is the dominant ion scale instability both in EC-only and mixed EC-NB heated discharges, with decreased growth-rates at $\delta < 0$ consistent with results exposed in Sec. 3.2 [83]. Nevertheless, the use of both beam heating and the more collisional regime in which the DIII-D discharges were operated even in the EC-only heated phase, as compared to the collisionless discharges on TCV, lowered the T_e/T_i ratio: this caused ETG modes to be linearly unstable even in the core, whereas modeling of the TCV discharges indicated no such feature [163, 171].

The impurity confinement time was estimated by ablating suitable Aluminium targets using the Laser Blow-Off system, yielding a particle to energy confinement time ratio, τ_P/τ_E, of order unity [83]. As opposed to H-mode regimes, for which such ratio is typi-
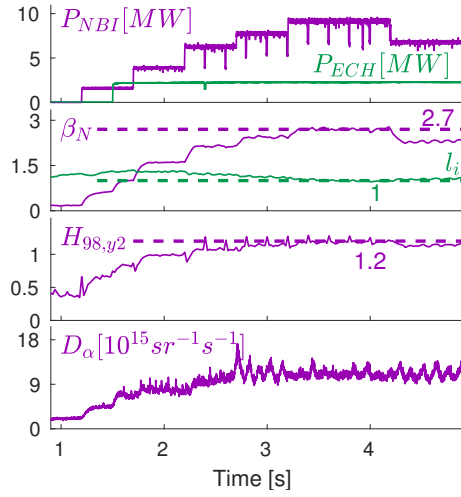
Fig. 15 Time evolution of DIII-D discharge #176283. From top to bottom, auxiliary power (NBI-ECH), normalized pressure β_N and internal inductance l_i, confinement enhancement factor $H_{98,y2}$, D_α signal (Reproduced from [83], with the permission of AIP Publishing).

cally measured in the range $2-4$, this scenario makes impurity retention less problematic although fueling might be more difficult in large devices depending on how the main ion particle transport scales compared to that of impurities. The low τ_P/τ_E value is believed to be due to the absence of a density edge barrier, rather than to the negative value of triangularity, as it is consistent with results in the I-mode regime [184]. The intensity of fluctuations was monitored by the phase contrast imaging [185] (PCI), the beam emission spectroscopy [186] (BES) and the CECE [187] diagnostics. All systems consistently detected a decreased intensity of fluctuations in $\delta < 0$ plasmas as compared to matched $\delta > 0$ discharges at fixed conditions, consistent with lower transport coefficients [83]. While the radial dependence of the reduction of the intensity of fluctuations appears to differ between the BES and CECE systems (see Figure 5 of [83]), no dedicated study was executed trying to determine whether the beneficial effect of $\delta < 0$ on the intensity of fluctuations is uniform across the minor radius or decreases towards the axis following the finite penetration length of triangularity. As a consequence, due to the paucity of data for which both the BES and the CECE systems were simultaneously measuring the same plasma region with good signal to noise ratio, it is not possible to determine whether the observed difference is real or, rather, is an artifact caused by uncertainties in the measurements.

4 Energetic particles

In order to assess whether a given cross sectional shape is beneficial for confinement, its impact on the transport coefficients must be evaluated both for thermal and for supra-thermal species. Indeed, if fast ion modes caused enhanced anomalous transport in $\delta < 0$ plasmas, this could potentially reduce the impact of the turbulence stabilization discussed in Sec. 3.1.

At present, only one published work [188], whose main findings are summarized hereafter, has reported on a DIII-D experiment dedicated to fast ion physics in $\delta < 0$ plasmas. Inner-wall limited (IWL) plasmas with opposite values of triangularity were compared

while holding actuators such as line averaged density ($\langle n_e \rangle$), plasma current (I_P), toroidal field (B_T) and auxiliary power the same. Fast ion modes were probed using beam heating during the current ramp-up phase, which is the reference scenario used on DIII-D [189] for fast ion studies because it slows down the current penetration, thereby creating a region with reverse magnetic shear, and generates a good fraction of energetic ions. The discharge evolution is such that the LCFS in plasmas at $\delta > 0$ converges more slowly to its final form than its $\delta < 0$ counterpart, resulting in 12% larger elongation for the former. All experiments reported in the DIII-D work were carried out with $B_T = 2.0\,\mathrm{T}$, $\langle n_e \rangle < 5 \times 10^{19}\,\mathrm{m}^{-3}$, $I_P < 1\,\mathrm{MA}$ as well as electron and ion temperatures below 5 keV. All $\delta < 0$ plasmas with early beam heating display numerous Alfvén eigenmodes (AE), including Beta induced Alfvén Acoustic Eigenmodes (BAAEs) [190], Beta induced Alfvén Eigenmodes (BAEs) [191], Reversed Shear Alfvén Eigenmodes (RSAEs) [192] and Toroidicity induced Alfvén Eigenmodes (TAEs) [193]. The number of unstable Alfvén modes as well as their amplitude was found to increases in power scans, as expected. Additionally, the amplitude of the AE is quantitatively comparable between the two shapes, consistent with the fact that, although the fraction of thermal particles that are trapped is larger in $\delta < 0$ configurations, the fraction of fast ions that are trapped does not significantly depend on triangularity. However, as displayed in Fig. 16, many of the modes in $\delta < 0$ plasmas, especially BAEs and RSAEs, feature a quasi-coherent or chirping frequency evolution which, on DIII-D, is more typically found in H-mode plasmas. Some authors argue that such behavior is attributable to a lower intensity of fluctuations in the background plasma which, by decreasing the amount of stochastic scattering energetic particles are subject to, allows coherent structures in phase space to shine through the background noise [194]. Values of fast ion transport were deduced using a dedicated beam modulation technique [195] and comparing the corresponding response measured by fast ion diagnostics to that expected by classical calculations from the TRANSP code [196]. The measured modulated neutron emission signal departs from the TRANSP predictions at increasing auxiliary beam power, consistent with the fact that AEs trasnport beam ions faster than the classical expectations. However, by comparing the inferred transport levels of $\delta < 0$ discharges to those computed for oval plasmas at similar values of auxiliary power, no dependence on triangularity was found despite a large difference in the spectra; this could be a manifestation of the fact that local fast ion gradients relax to a marginally unstable value [188]. Based on such findings, at least in the cases examined, fast ion transport does not appear to worsen at $\delta < 0$. As a result, the improved thermal confinement displayed by $\delta < 0$ plasmas is not expected to be deteriorated by the fast ion population in a greater amount than the $\delta > 0$ counterpart.

Fast ions losses entail a number of potential issues in any tokamak, both under safe operation and physics standpoints, and are briefly discussed below. In order to establish safe protocols for operation in $\delta < 0$ plasmas, prompt losses were predicted in [188] to be quantitatively similar between the two IWL shapes at $\delta < 0$ and $\delta > 0$ to be run on DIII-D, although differences were found in the region of the vessel in which power would be deposited. More recently, ion orbit losses were computed in the case of double-null diverted configurations in [125], where it was found that, in contrast to $\delta > 0$ plasmas in which fast ions typically complete their banana orbits, $\delta < 0$ plasmas are expected to suffer from enhanced losses primarily due to the X-point diverting trapped fast ions to the inner plate. The subsequent creation of edge electric fields is argued to inhibit the formation of H-mode pedestals in diverted $\delta < 0$ configurations. This mechanism, however, would not explain the higher L→H power threshold observed in IWL $\delta < 0$ configurations when compared to $\delta > 0$ counterparts [83].
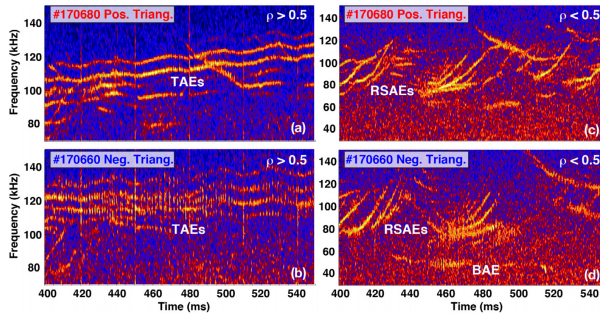
Fig. 16 ECE spectrograms displaying the time evolution of a variety of Alfvén modes in the current ramp-up phase of $\delta > 0$ DIII-D discharge #170680 (a-c) and $\delta < 0$ discharge #170660 (b-d). (Reproduced from [188], with the permission of IAEA Publishing).

5 Power exhaust

Comparatively little work has been performed to date on characterizing the power exhaust properties of negative-triangularity plasmas. In fact, to our knowledge there is a single published article on the subject, which examined some features of this issue in TCV [197].

This work focused on the SOL power fall-off length, λ_q, and in particular on its dependence on triangularity in L-mode. The scenario used in this study featured a lower-single-null diverted shape with lower positive triangularity and varying upper triangularity δ_{up}, from -0.28 to 0.47. The value of λ_q at the outer target was found to decrease monotonically with δ_{up} going from positive to negative, independently of the direction of the magnetic ∇B drift and of the main ion species being deuterium or helium. By contrast, the *inner* power fall-off length features a maximum at $\delta_{up} \sim 0$ and decreases with finite triangularity of either sign [197].

The value of λ_q, particularly at the outer target which generally features a larger heat flux, is of great importance in a reactor as it directly affects the heat load on a reactor's first wall, smaller values being increasingly worrisome. The decrease of the outer fall-off length with negative triangularity can thus be seen as a detrimental effect. However, the values of power fall-off lengths are related to the spatial scale lengths of pressure profiles which, in turn, are set by the turbulence levels for a given flux. As such, $\delta < 0$ discharges with improved confinement over matched $\delta > 0$ counterparts are characterized by shorter λ_q. However, the TCV team reported that $\delta < 0$ L-mode plasmas with H-mode grade confinement are characterized by wider λ_q [197] than $\delta > 0$ plasmas with comparable core performance [198]. Similarly, it has been recently reported on DIII-D that the SOL power fall-off length in $\delta < 0$ L-mode plasmas characterized by H-mode grade confinement and pressure levels ($H_{98,y2} \simeq 1$, $\beta_N \simeq 3$) exceeds by 50% values from the ITPA scaling law [199]. This result is understood by considering that, as explained above, λ_q widens with stronger turbulence near the edge, as is typically measured in L-mode vs H-mode plasmas. When evaluating the requirements relative to exhaust power in L-mode $\delta < 0$ vs H-mode $\delta > 0$ plasmas, for similar values of global confinement, such observations add further to the merits of the former scenario vs the latter.

To conclude, we note that $\delta < 0$ plasmas are also particularly attractive from a power exhaust stand-point because the strike points naturally impinge on the divertor on the low field side of the machine. As such, for a given value of λ_q on at the separatrix, the heat flux

foot print is wider than that in $\delta > 0$ counterparts by the ratio of the major radii at which strike points impinge on the divertor in these two configurations.

Conclusions and future perspectives

The negative-triangularity tokamak is a concept that has existed for over five decades and has been actively explored experimentally for twenty-five years. Yet, in some ways it can be said to be in its infancy because, for most of this time, it has been a fringe configuration studied as little more than a curiosity from a theoretical standpoint and investigated experimentally with perseverance only on the TCV tokamak.

Indeed, based on initial MHD estimates, plasmas at negative triangularity were not expected to achieve reactor relevant pressure levels. Furthermore, although early experiments did succeed in controlling NT plasmas [50,151,51]), plasmas were most probably too collisional and not sufficiently triangular, or elongated, to observe the confinement improvement that was much later obtained on TCV and DIII-D [157,82]. As such, negative triangularity plasmas, along with other non standard configurations like the bean-shaped [104], could not compete with promising results obtained in standard-dee plasmas. The discovery of the H-mode regime [21], which happened at about the same time, understandably steered the fusion community towards configurations at positive triangularity.

As the realm of energy and particle confinement began to be experimentally explored and theoretically developed, it was realized that tokamak performances are mostly curtailed by confinement properties and density limits, rather than by ideal MHD boundaries, obviously provided the latter are above the target equilibria. Thus, between the counteracting properties of better confinement and decreased stability in NT plasmas, the former began to have a dominant role. High β equilibria that benefited from an improved confinement due to stabilization of micro-instabilities from banana tips being in the good curvature region were proposed in the mid-1990s [200,76,144], but failed to attract vast interest worldwide.

Only with the recent development of integrated scenarios that need to simultaneously optimize all aspects of a reactor, from pressure levels sustained in the core to wall exhaust, has the fusion community started to realize the immense challenges that a reactor based on conventional scenarios will face. Indeed, an *optimal* design of a reactor should by definition be near all the related limits, taking into account the respective risks, and should not favor a particular parameter, e.g. MHD limit with respect to exhaust. Consequently, the need for alternative options for DEMO has lately caused a decisive paradigm shift in how negative triangularity is perceived by the fusion community. The important additional contributions of DIII-D and the very recent developments on HL-2M [62] and on ASDEX Upgrade [201] bear witness to a renewed worldwide interest and the option of a negative-triangularity reactor is now being looked at very seriously indeed [35].

There is every reason to believe that the coming decade will see rapid progress towards a thorough characterization of the negative-triangularity tokamak concept, and bring us close to a proper reactor feasibility assessment.

Conflict of interest

The authors declare that they have no conflict of interest.

References

1. V. Shafranov, Journal of the Russian Academy of Sciences **44**(8), 835 (2001). DOI DOI:10.1070/PU2001v044n08ABEH001068
2. M. Kruskal, R. Kulsrud, The Physics of Fluids **1**(4), 265 (1958). DOI 10.1063/1.1705884. URL https://aip.scitation.org/doi/abs/10.1063/1.1705884
3. L. Solovev, V. Shafranov, E. Yurchenko, in *Plasma Physics and Controlled Nuclear Fusion Research* (International Atomic Energy Agency, 1969), p. 175
4. G. Laval, H. Luc, E. Maschke, C. Mercier, R. Pellat, in *Plasma Physics and Controlled Nuclear Fusion Research* (International Atomic Energy Agency, 1971), p. 507
5. B. Coppi, R. Dagazian, R. Gajewski, The Physics of Fluids **15**(12), 2405 (1972). DOI 10.1063/1.1693885. URL https://aip.scitation.org/doi/abs/10.1063/1.1693885
6. L. Artsimovich, V. Shafranov, JETP Lett. **15**(1), 51 (1972)
7. V. Shafranov, Sov. Phys.-Tech. Phys. (Engl. Transl.) **15**, 175 (1970). URL https://www.osti.gov/biblio/4079592
8. T. Ohkawa, H.G. Voorhies, Phys. Rev. Lett. **22**, 1275 (1969). DOI 10.1103/PhysRevLett.22.1275. URL https://link.aps.org/doi/10.1103/PhysRevLett.22.1275
9. H.P. Furth, Plasma Physics and Controlled Fusion **28**(9A), 1305 (1986). DOI 10.1088/0741-3335/28/9a/009. URL https://doi.org/10.1088/0741-3335/28/9a/009
10. B. Coppi, Comments Plasma Phys. and Cont. Fusion **5**, 261 (1980)
11. C. Mercier, in *VII Conference in Plasma Physics and Controlled Nuclear Fusion Research, Innsbruck* (International Atomic Energy Agency, 1978), pp. 701, IAEA/CN37 P.3–2
12. D. Lortz, J. Nührenberg, Physics Letters A **68**(1), 49 (1978). DOI https://doi.org/10.1016/0375-9601(78)90753-3. URL http://www.sciencedirect.com/science/article/pii/0375960178907533
13. B. Coppi, A. Ferreira, J.J. Ramos, Phys. Rev. Lett. **44**, 990 (1980). DOI 10.1103/PhysRevLett.44.990. URL https://link.aps.org/doi/10.1103/PhysRevLett.44.990
14. R.E. Bell, N. Asakura, S. Bernabei, M.S. Chance, P. Duperrex, R.J. Fonck, G.M. Gammel, G. Greene, R.E. Hatcher, A. Holland, S.C. Jardin, T. Jiang, R. Kaita, S.M. Kaye, C.E. Kessel, H.W. Kugel, B. LeBlanc, F.M. Levinton, M. Okabayashi, M. Ono, S.F. Paul, E.T. Powell, Y. Qin, D.W. Roberts, N.R. Sauthoff, S. Sesnic, H. Takahashi, Physics of Fluids B: Plasma Physics **2**(6), 1271 (1990). DOI 10.1063/1.859542. URL https://doi.org/10.1063/1.859542
15. J. File, R.G. Mills, G.V. Sheffield, IEEE Transactions on Nuclear Science **18**(4), 277 (1971). DOI 10.1109/TNS.1971.4326354
16. W. Gray, W. Stoddart, J. Akin, Bending free toroidal shells for tokamak fusion reactors. Tech. rep., Oak Ridge National Laboratory (1974)
17. F. Troyon, A, W.A. Cooper, F. Yasseen, A. Turnbull, Plasma Physics and Controlled Fusion **30**(11), 1597 (1988). DOI 10.1088/0741-3335/30/11/019. URL https://doi.org/10.1088/0741-3335/30/11/019
18. Y. Neyatani, the JT-60 Team, Plasma Physics and Controlled Fusion **38**(12A), A181 (1996). DOI 10.1088/0741-3335/38/12a/014. URL https://doi.org/10.1088/0741-3335/38/12a/014
19. T.S. Taylor, Plasma Physics and Controlled Fusion **39**(12B), B47 (1997). DOI 10.1088/0741-3335/39/12b/005. URL https://doi.org/10.1088/0741-3335/39/12b/005
20. T. Hender, J. Wesley, J. Bialek, A. Bondeson, A. Boozer, R. Buttery, A. Garofalo, T. Goodman, R. Granetz, Y. Gribov, O. Gruber, M. Gryaznevich, G. Giruzzi, S. Günter, N. Hayashi, P. Helander, C. Hegna, D. Howell, D. Humphreys, G. Huysmans, A. Hyatt, A. Isayama, S. Jardin, Y. Kawano, A. Kellman, C. Kessel, H. Koslowski, R.L. Haye, E. Lazzaro, Y. Liu, V. Lukash, J. Manickam, S. Medvedev, V. Mertens, S. Mirnov, Y. Nakamura, G. Navratil, M. Okabayashi, T. Ozeki, R. Paccagnella, G. Pautasso, F. Porcelli, V. Pustovitov, V. Riccardo, M. Sato, O. Sauter, M. Schaffer, M. Shimada, P. Sonato, E. Strait, M. Sugihara, M. Takechi, A. Turnbull, E. Westerhof, D. Whyte, R. Yoshino, H. Zohm, D. the ITPA MHD, M. Group, Nuclear Fusion **47**(6), S128 (2007). DOI 10.1088/0029-5515/47/6/s03. URL https://doi.org/10.1088/0029-5515/47/6/s03

21. F. Wagner, G. Becker, K. Behringer, D. Campbell, A. Eberhagen, W. Engelhardt, G. Fussmann, O. Gehre, J. Gernhardt, G.v. Gierke, G. Haas, M. Huang, F. Karger, M. Keilhacker, O. Klüber, M. Kornherr, K. Lackner, G. Lisitano, G.G. Lister, H.M. Mayer, D. Meisel, E.R. Müller, H. Murmann, H. Niedermeyer, W. Poschenrieder, H. Rapp, H. Röhr, F. Schneider, G. Siller, E. Speth, A. Stäbler, K.H. Steuer, G. Venus, O. Vollmer, Z. Yü, Phys. Rev. Lett. **49**, 1408 (1982). DOI 10.1103/PhysRevLett.49.1408. URL https://link.aps.org/doi/10.1103/PhysRevLett.49.1408

22. H. Biglari, P.H. Diamond, P.W. Terry, Physics of Fluids B: Plasma Physics **2**(1), 1 (1990). DOI 10.1063/1.859529. URL https://doi.org/10.1063/1.859529

23. K.H. Burrell, Physics of Plasmas **4**(5), 1499 (1997). DOI 10.1063/1.872367. URL https://doi.org/10.1063/1.872367

24. H.R. Wilson, P.B. Snyder, G.T.A. Huysmans, R.L. Miller, Physics of Plasmas **9**(4), 1277 (2002). DOI 10.1063/1.1459058. URL https://doi.org/10.1063/1.1459058

25. S.I. Krasheninnikov, A.S. Kukushkin, Journal of Plasma Physics **83**(5), 155830501 (2017). DOI 10.1017/S0022377817000654

26. V.A. Soukhanovskii, Plasma Physics and Controlled Fusion **59**(6), 064005 (2017). DOI 10.1088/1361-6587/aa6959. URL https://doi.org/10.1088/1361-6587/aa6959

27. A. McLean, A. Leonard, M. Makowski, M. Groth, S. Allen, J. Boedo, B. Bray, A. Briesemeister, T. Carlstrom, D. Eldon, M. Fenstermacher, D. Hill, C. Lasnier, C. Liu, T. Osborne, T. Petrie, V. Soukhanovskii, P. Stangeby, C. Tsui, E. Unterberg, J. Watkins, Journal of Nuclear Materials **463**, 533 (2015). DOI https://doi.org/10.1016/j.jnucmat.2015.01.066. URL http://www.sciencedirect.com/science/article/pii/S0022311515000835. PLASMA-SURFACE INTERACTIONS 21

28. H. Du, G. Zheng, H. Guo, A.E. Jaervinen, X. Duan, X. Bonnin, D. Eldon, D. Wang, Nuclear Fusion **60**(4), 046028 (2020). DOI 10.1088/1741-4326/ab77e6. URL https://doi.org/10.1088/1741-4326/ab77e6

29. A. Loarte, G. Huijsmans, S. Futatani, L. Baylor, T. Evans, D.M. Orlov, O. Schmitz, M. Becoulet, P. Cahyna, Y. Gribov, A. Kavin, A.S. Naik, D. Campbell, T. Casper, E. Daly, H. Frerichs, A. Kischner, R. Laengner, S. Lisgo, R. Pitts, G. Saibene, A. Wingen, Nuclear Fusion **54**(3), 033007 (2014). DOI 10.1088/0029-5515/54/3/033007. URL https://doi.org/10.1088/0029-5515/54/3/033007

30. P. Lang, A. Loarte, G. Saibene, L. Baylor, M. Becoulet, M. Cavinato, S. Clement-Lorenzo, E. Daly, T. Evans, M. Fenstermacher, Y. Gribov, L. Horton, C. Lowry, Y. Martin, O. Neubauer, N. Oyama, M. Schaffer, D. Stork, W. Suttrop, P. Thomas, M. Tran, H. Wilson, A. Kavin, O. Schmitz, Nuclear Fusion **53**(4), 043004 (2013). DOI 10.1088/0029-5515/53/4/043004. URL https://doi.org/10.1088/0029-5515/53/4/043004

31. S. Medvedev, M. Kikuchi, L. Villard, T. Takizuka, P. Diamond, H. Zushi, K. Nagasaki, X. Duan, Y. Wu, A. Ivanov, A. Martynov, Y. Poshekhonov, A. Fasoli, O. Sauter, Nuclear Fusion **55**(6), 063013 (2015). DOI 10.1088/0029-5515/55/6/063013. URL https://doi.org/10.1088/0029-5515/55/6/063013

32. A. Turnbull, A. Roy, O. Sauter, F. Troyon, Nuclear Fusion **28**(8), 1379 (1988). DOI 10.1088/0029-5515/28/8/006. URL https://doi.org/10.1088/0029-5515/28/8/006

33. O. Sauter, Fusion Engineering and Design **112**, 633 (2016). DOI 10.1016/j.fusengdes.2016.04.033. URL https://www.sciencedirect.com/science/article/pii/S0920379616303234

34. R.L. Miller, M.S. Chu, J.M. Greene, Y.R. Lin-Liu, R.E. Waltz, Physics of Plasmas **5**(4), 973 (1998). DOI 10.1063/1.872666. URL https://doi.org/10.1063/1.872666

35. M. Kikuchi, T. Takizuka, S. Medvedev, T. Ando, D. Chen, J. Li, M. Austin, O. Sauter, L. Villard, A. Merle, M. Fontana, Y. Kishimoto, K. Imadera, Nuclear Fusion **59**(5), 056017 (2019). DOI 10.1088/1741-4326/ab076d. URL https://doi.org/10.1088/1741-4326/ab076d

36. M. Kikuchi, S. Medvedev, T. Takizuka, A. Fasoli, Y. Wu, P. Diamond, X. Duan, Y. Kishimoto, K. Hanada, L. Villard, O. Sauter, S. Coda, B. Duval, H. Reimerdes, S. Brunner, G. Merlo, J. Jiang, M. Wang, M. Ni, D. Chen, H. Du, W. Duan, Y. Hou, A. Ivanov, A. Martynov, Y. Poshekhonov, Y. Ueda, L. Yan, X. Song, G. Zheng, J. Liu, K. Nagasaki, K. Imadera, K. Mishra, A. Fujisawa, K. Nakamura, H. Zushi, M.J. Pueschel, X.Z. Xu, P. hu, D. Told, G.Q. Li, M. Furukawa, T. Ozeki, K. Shimizu, K. Kawashima, H. Urano, M. Honda, T. Ando, M. Kuriyama, 42nd EPS Conference on Plasma Physics **1**(1), P4.179 (2015). URL http://ocs.ciemat.es/EPS2015PAP/pdf/P4.179.pdf

37. M. Kikuchi, T. Takizuka, M. Furukawa, in *Proceedings of the 12th Asia Pacific Physics Conference (APPC12)* (2014), p. 015014. DOI 10.7566/JPSCP.1.015014. URL https://journals.jps.jp/doi/abs/10.7566/JPSCP.1.015014

38. M. Kikuchi, A. Fasoli, T. Takizuka, P. Diamond, S.Y. Medvedev, X. Duan, H. Zushi, M. Furukawa, Y. Kishimoto, Y. Wu, O. Sauter, L. Villard, S. Brunner, G. Merlo, G. Zheng, K. Mishra, M. Honda, H. Urano, M. Pueschel, D. Told, A. Fujisawa, K. Nagasaki, F. Sano, in *1st Int. E-Conf. on Energies (March 2014)* (2014), p. E002. DOI 10.3390/ece-1-e002. URL http://sciforum.net/conference/ece-1/paper/2321

39. E. Rebhan, Nuclear Fusion **15**(2), 277 (1975). DOI 10.1088/0029-5515/15/2/012. URL https://doi.org/10.1088/0029-5515/15/2/012

40. E. Rebhan, A. Salat, Nuclear Fusion **16**(5), 805 (1976). DOI 10.1088/0029-5515/16/5/009. URL https://doi.org/10.1088/0029-5515/16/5/009

41. E. Rebhan, A. Salat, Nuclear Fusion **17**(2), 251 (1977). DOI 10.1088/0029-5515/17/2/008. URL https://doi.org/10.1088/0029-5515/17/2/008

42. E. Rebhan, A. Salat, Nuclear Fusion **18**(10), 1431 (1978). DOI 10.1088/0029-5515/18/10/011. URL https://doi.org/10.1088/0029-5515/18/10/011

43. L. Solov'ev, Sov. Phys. JETP **26**(2), 400 (1968)

44. L. Bernard, D. Berger, R. Gruber, F. Troyon, Nuclear Fusion **18**(10), 1331 (1978). DOI 10.1088/0029-5515/18/10/001. URL https://doi.org/10.1088/0029-5515/18/10/001

45. R. Gruber, Journal of Computational Physics **26**(3), 379 (1978). DOI https://doi.org/10.1016/0021-9991(78)90076-1. URL https://www.sciencedirect.com/science/article/pii/0021999178900761

46. M. Chu, R.L. Miller, The Physics of Fluids **21**(5), 817 (1978). DOI 10.1063/1.862300. URL https://aip.scitation.org/doi/abs/10.1063/1.862300

47. K. Yamazaki, H. Fishman, M. Okabayashi, A.M.M. Todd, Plasma Physics **25**(11), 1245 (1983). DOI 10.1088/0032-1028/25/11/005. URL https://doi.org/10.1088/0032-1028/25/11/005

48. R.C. Grimm, J.M. Greene, J.L. Johnson, in *Controlled Fusion*, *Methods in Computational Physics: Advances in Research and Applications*, vol. 16, ed. by J. Killeen (Elsevier, 1976), pp. 253–280. DOI https://doi.org/10.1016/B978-0-12-460816-0.50012-9. URL https://www.sciencedirect.com/science/article/pii/B9780124608160500129

49. B. Lipschultz, S. Prager, A. Todd, J. Delucia, Nuclear Fusion **20**(6), 683 (1980). DOI 10.1088/0029-5515/20/6/004. URL https://doi.org/10.1088/0029-5515/20/6/004

50. B. Lipschultz, S.C. Prager, T.H. Osborne, J.C. Sprott, M. Phillips, Phys. Rev. Lett. **43**, 36 (1979). DOI 10.1103/PhysRevLett.43.36. URL https://link.aps.org/doi/10.1103/PhysRevLett.43.36

51. H. Takahashi, K. Bol, H. Maeda, M. Okabayashi, M. Reusch, Nuclear Fusion **22**(12), 1597 (1982). DOI 10.1088/0029-5515/22/12/006. URL https://doi.org/10.1088/0029-5515/22/12/006

52. J. Akkermans, Physica B+C **115**(1), 103 (1982). DOI https://doi.org/10.1016/0378-4363(82)90060-2. URL https://www.sciencedirect.com/science/article/pii/0378436382900602

53. D. Ward, S. Jardin, C. Cheng, Journal of Computational Physics **104**(1), 221 (1993)

54. C. Cheng, M. Chance, Journal of Computational Physics **71**(1), 124 (1987). DOI https://doi.org/10.1016/0021-9991(87)90023-4. URL https://www.sciencedirect.com/science/article/pii/0021999187900234

55. D. Ward, A. Bondeson, F. Hofmann, Nuclear Fusion **33**(5), 821 (1993). DOI 10.1088/0029-5515/33/5/i12. URL https://doi.org/10.1088/0029-5515/33/5/i12

56. L. Degtyarev, A. Martynov, S. Medvedev, F. Troyon, L. Villard, R. Gruber, Computer Physics Communications **103**(1), 10 (1997). DOI https://doi.org/10.1016/S0010-4655(97)00037-4. URL https://www.sciencedirect.com/science/article/pii/S0010465597000374

57. S.Y. Medvedev, A.A. Ivanov, A.A. Martynov, Y.Y. Poshekhonov, R. Behn, Y.R. Martin, A. Pochelon, O. Sauter, L. Villard, 35th EPS Conference on Plasma Phys. Hersonissos, 9 - 13 June 2008 ECA **32D**, P (2008). URL http://epsppd.epfl.ch/Hersonissos/pdf/P1072.pdf

58. S.Y. Medvedev, A.A. Ivanov, A.A. Martynov, Y.Y. Poshekhonov, Y.R. Martin, J.M. Moret, F. Piras, A. Pitzschke, A. Pochelon, O. Sauter, L. Villard, the TCV team, 36th EPS Conference on Plasma Phys. Sofia, June 29 - July 3, 2009 ECA **33E**, P (2009). URL http://epsppd.epfl.ch/Sofia/pdf/P2143.pdf

59. S.Y. Medvedev, A. Ivanov, A. Martynov, Y. Poshekhonov, M. Kikuchi, A. Pochelon, H. Reimerdes, O. Sauter, L. Villard, et al., in *Europhysics Conference Abstracts* (European Physical Society, 2014), P4-039

60. D. Abate, G. Marchiori, P. Bettini, F. Villone, Plasma Physics and Controlled Fusion **62**(8), 085001 (2020). DOI 10.1088/1361-6587/ab93a5. URL https://doi.org/10.1088/1361-6587/ab93a5

61. R. Khayrutdinov, V. Lukash, Journal of Computational Physics **109**(2), 193 (1993). DOI https://doi.org/10.1006/jcph.1993.1211. URL https://www.sciencedirect.com/science/article/pii/S0021999183712118

62. L. Xue, G.Y. Zheng, X.R. Duan, Y.Q. Liu, G.T. Hoang, J.X. Li, V.N. Dokuka, V.E. Lukash, R.R. Khayrutdinov, Fusion Engineering and Design **143**, 48 (2019). DOI 10.1016/j.fusengdes.2019.03.103. URL https://www.sciencedirect.com/science/article/pii/S0920379619304363

63. J.W. Connor, R.J. Hastie, J.B. Taylor, Phys. Rev. Lett. **40**, 396 (1978). DOI 10.1103/PhysRevLett.40.396. URL https://link.aps.org/doi/10.1103/PhysRevLett.40.396

64. G. Federici, R. Kemp, D. Ward, C. Bachmann, T. Franke, S. Gonzalez, C. Lowry, M. Gadomska, J. Harman, B. Meszaros, C. Morlock, F. Romanelli, R. Wenninger, Fusion Engineering and Design **89**(7), 882 (2014). DOI https://doi.org/10.1016/j.fusengdes.2014.01.070. URL https://www.sciencedirect.com/science/article/pii/S0920379614000714. Proceedings of the 11th International Symposium on Fusion Nuclear Technology-11 (ISFNT-11) Barcelona, Spain, 15-20 September, 2013

65. C.E. Kessel, F.M. Poli, Fusion Science and Technology **67**(1), 220 (2015). DOI 10.13182/FST14-793. URL https://doi.org/10.13182/FST14-793

66. B. Sorbom, J. Ball, T. Palmer, F. Mangiarotti, J. Sierchio, P. Bonoli, C. Kasten, D. Sutherland, H. Barnard, C. Haakonsen, J. Goh, C. Sung, D. Whyte, Fusion Engineering and Design **100**, 378 (2015). DOI https://doi.org/10.1016/j.fusengdes.2015.07.008. URL https://www.sciencedirect.com/science/article/pii/S0920379615302337

67. R.J. Buttery, J.M. Park, J.T. McClenaghan, D. Weisberg, J. Canik, J. Ferron, A. Garofalo, C.T. Holcomb, J. Leuer, P.B. Snyder, Nuclear Fusion **61**(4), 046028 (2021). DOI 10.1088/1741-4326/abe4af. URL https://doi.org/10.1088/1741-4326/abe4af

68. J.W. Connor, R.J. Hastie, H.R. Wilson, R.L. Miller, Physics of Plasmas **5**, 2687 (1998). DOI 10.1063/1.872956. URL https://doi.org/10.1063/1.872956

69. T. Ohkawa, Kakuyugo-Kenkyu **22**(2), 99 (1969). DOI 10.1585/jspf1958.22.99

70. K. Yamazaki, Japanese Journal of Applied Physics **19**(5), 963 (1980)

71. C. Mercier, Nuclear Fusion **1**, 47; Nucl. Fusion Suppl. 2 (1962) 801 (1960). DOI 10.1088/0029-5515/1/1/004. URL https://doi.org/10.1088/0029-5515/1/1/004;Nucl.FusionSuppl.2(1962)801

72. H. Lutjens, A. Bondeson, G. Vlad, Nuclear Fusion **32**(9), 1625 (1992). DOI 10.1088/0029-5515/32/9/i10. URL https://doi.org/10.1088/0029-5515/32/9/i10

73. R. Galvão, Nuclear Fusion **15**(5), 785 (1975). DOI 10.1088/0029-5515/15/5/008. URL https://doi.org/10.1088/0029-5515/15/5/008

74. H.R. Wilson, R.L. Miller, Physics of Plasmas **6**(3), 873 (1999). DOI 10.1063/1.873326. URL https://doi.org/10.1063/1.873326

75. H. Reimerdes, A. Pochelon, O. Sauter, T.P. Goodman, M.A. Henderson, A. Martynov, Plasma Physics and Controlled Fusion **42**(6), 629 (2000). DOI 10.1088/0741-3335/42/6/302. URL https://doi.org/10.1088/0741-3335/42/6/302

76. T. Ohkawa, V. Chan, M. Chu, R. Dominguez, R. Miller, Nucl. Fusion Suppl., in Plasma Physics and Controlled Nuclear Fusion Research 1989 (Proc. 12th Int. Conf. Nice, 1988), IAEA, Vienna **1**, 681, IAEA (1989)

77. A. Wootton, Nuclear Fusion **18**(8), 1161 (1978). DOI 10.1088/0029-5515/18/8/007. URL https://doi.org/10.1088/0029-5515/18/8/007

78. Y.K. Peng, R. Dory, D. Nelson, R. Sayer, The Physics of Fluids **21**(3), 467 (1978)

79. F. Troyon, R. Gruber, H. Saurenmann, S. Semenzato, S. Succi, Plasma Physics and Controlled Fusion **26**(1A), 209 (1984). DOI 10.1088/0741-3335/26/1a/319. URL https://doi.org/10.1088/0741-3335/26/1a/319

80. F. Troyon, R. Gruber, Physics Letters A **110**(1), 29 (1985). DOI https://doi.org/10.1016/0375-9601(85)90227-0. URL https://www.sciencedirect.com/science/article/pii/0375960185902270

81. F. Hofmann, B. Marcus, A. Perez, A. Turnbull, S. Jardin, in *Fusion Technology 1986* (Pergamon, 1986), pp. 687–692. DOI https://doi.org/10.1016/B978-1-4832-8376-0.50085-1. URL https://www.sciencedirect.com/science/article/pii/B9781483283760500851

82. M.E. Austin, A. Marinoni, M.L. Walker, M.W. Brookman, J.S. deGrassie, A.W. Hyatt, G.R. McKee, C.C. Petty, T.L. Rhodes, S.P. Smith, C. Sung, K.E. Thome, A.D. Turnbull, Phys. Rev. Lett. **122**, 115001 (2019). DOI 10.1103/PhysRevLett.122.115001. URL https://link.aps.org/doi/10.1103/PhysRevLett.122.115001

83. A. Marinoni, M.E. Austin, A.W. Hyatt, M.L. Walker, J. Candy, C. Chrystal, C.J. Lasnier, G.R. McKee, T. Odstrčil, C.C. Petty, M. Porkolab, J.C. Rost, O. Sauter, S.P. Smith, G.M. Staebler, C. Sung, K.E. Thome, A.D. Turnbull, L. Zeng, Physics of Plasmas **26**(4), 042515 (2019). DOI 10.1063/1.5091802. URL https://doi.org/10.1063/1.5091802

84. F. Porcelli, M.N. Rosenbluth, Plasma Physics and Controlled Fusion **40**(4), 481 (1998). DOI 10.1088/0741-3335/40/4/004. URL https://doi.org/10.1088/0741-3335/40/4/004

85. H. Lütjens, A. Bondeson, O. Sauter, Computer physics communications **97**(3), 219 (1996)

86. H.G. Eriksson, C. Wahlberg, Physics of Plasmas **9**(5), 1606 (2002). DOI 10.1063/1.1464890. URL https://doi.org/10.1063/1.1464890

87. A. Martynov, J.P. Graves, O. Sauter, Plasma Physics and Controlled Fusion **47**(10), 1743 (2005). DOI 10.1088/0741-3335/47/10/009. URL https://doi.org/10.1088/0741-3335/47/10/009

88. J.P. Graves, C. Angioni, R.V. Budny, R.J. Buttery, S. Coda, L.G. Eriksson, C.G. Gimblett, T.P. Goodman, R.J. Hastie, M.A. Henderson, H.R. Koslowski, M.J. Mantsinen, A. Martynov, M.L. Mayoral, A. Mück, M.F.F. Nave, O. Sauter, E. Westerhof, J. Contributors, Plasma Physics and Controlled Fusion **47**(12B), B121 (2005). DOI 10.1088/0741-3335/47/12b/s10. URL `https://doi.org/10.1088/0741-3335/47/12b/s10`

89. J. Greene, M. Chance, Nuclear Fusion **21**(4), 453 (1981). DOI 10.1088/0029-5515/21/4/002. URL `https://doi.org/10.1088/0029-5515/21/4/002`

90. J. Manickam, Journal of Computational Physics **66**(2), 324 (1986)

91. C. Bishop, P. Kirby, J. Connor, R. Hastie, J. Taylor, Nuclear Fusion **24**(12), 1579 (1984). DOI 10.1088/0029-5515/24/12/006. URL `https://doi.org/10.1088/0029-5515/24/12/006`

92. C. Bishop, Nuclear Fusion **26**(8), 1063 (1986). DOI 10.1088/0029-5515/26/8/006. URL `https://doi.org/10.1088/0029-5515/26/8/006`

93. C. Bishop, Nuclear Fusion **27**(11), 1765 (1987). DOI 10.1088/0029-5515/27/11/002. URL `https://doi.org/10.1088/0029-5515/27/11/002`

94. JT-60 TEAM, Nucl. Fusion Suppl., in Plasma Physics and Controlled Nuclear Fusion Research 1986 (Proc. 1 lth Int. Conf. Kyoto, 1986), IAEA, Vienna, STIPUB723 **1**, 89 (1987)

95. A. Roy, F. Troyon, in Theory of Fusion Plasmas (Proc. Workshop held at Varenna, Italy, August 1987, A. Bondeson et al. Editors), Editrice Compositori, Bologna p. 143 (1988)

96. A. Roy, Stabilité MHD d'un tokamak quasi circulaire. optimisation des profils de courant et de pression et influence d'un point de rebroussement à la surface du plasma. Ph.D. thesis, Ecole Polytechnique Fédérale de Lausanne (EPFL), Lausanne (1990). DOI 10.5075/epfl-thesis-882. URL `https://infoscience.epfl.ch/record/31360`

97. L. Porte, J.A. Boedo, S. Brunner, S. Coda, M. Fontana, T. Golfinopoulos, W. Han, Z. Huang, B. Labit, A. Merle, G. Merlo, N. Offeddu, O. Sauter, C. Theiler, in 28th *IAEA Fusion Energy Conference* (International Atomic Energy Agency, 2020). URL `https://conferences.iaea.org/event/214/contributions/17841/`

98. A. Marinoni, M.E. Austin, A.W. Hyatt, S. Coda, J. Hanson, D. Pace, C. Paz-Soldan, C.C. Petty, M. Porkolab, T. Rhodes, F. Sciortino, F. Scotti, S. Smith, F. Turco, Z. Yan, in 28th *IAEA Fusion Energy Conference* (International Atomic Energy Agency, 2020). URL `https://conferences.iaea.org/event/214/contributions/17105/`

99. A. Merle, O. Sauter, S.Y. Medvedev, Plasma Physics and Controlled Fusion **59**(10), 104001 (2017). DOI 10.1088/1361-6587/aa7ac0. URL `https://doi.org/10.1088/1361-6587/aa7ac0`

100. A. Pochelon, P. Angelino, R. Behn, S. Brunner, S. Coda, N. Kirneva, S.Y. Medvedev, H. Reimerdes, J. Rossel, O. Sauter, L. Villard, D. Wagner, A. Bottino, Y. Camenen, G.P. Canal, P.K. Chattopadhyay, B.P. Duval, A. Fasoli, T.P. Goodman, S. Jolliet, A. Karpushov, B. Labit, A. Marinoni, J.M. Moret, A. Pitzschke, L. Porte, M. Rancic, V.S. Udintsev, the TCV Team, Plasma and Fusion Research **7**, 2502148 (2012). DOI 10.1585/pfr.7.2502148

101. M.S. Chance, S.C. Jardin, T.H. Stix, Phys. Rev. Lett. **51**, 1963 (1983). DOI 10.1103/PhysRevLett.51.1963. URL `https://link.aps.org/doi/10.1103/PhysRevLett.51.1963`

102. R. Grimm, M. Chance, A. Todd, J. Manickam, M. Okabayashi, W. Tang, R. Dewar, H. Fishman, S. Mendelsohn, D. Monticello, M. Phillips, M. Reusch, Nuclear Fusion **25**(7), 805 (1985). DOI 10.1088/0029-5515/25/7/005. URL `https://doi.org/10.1088/0029-5515/25/7/005`

103. J. Manickam, R.C. Grimm, M. Okabayashi, Phys. Rev. Lett. **51**, 1959 (1983). DOI 10.1103/PhysRevLett.51.1959. URL `https://link.aps.org/doi/10.1103/PhysRevLett.51.1959`

104. K. Bol, D. Buchenauer, M. Chance, P. Couture, H. Fishman, R. Fonck, G. Gammel, B. Grek, K. Ida, K. Itami, et al., Physical review letters **57**(15), 1891 (1986)

105. K. Yamazaki, T. Amano, H. Naitou, Y. Hamada, M. Azumi, Nuclear Fusion **25**(11), 1543 (1985). DOI 10.1088/0029-5515/25/11/003. URL `https://doi.org/10.1088/0029-5515/25/11/003`

106. A. Pochelon, F. Hofmann, H. Reimerdes, C. Angioni, R. Behn, R. Duquerroy, I. Furno, P. Gomez, T. Goodman, M. Henderson, A. Martynov, P. Nikkola, O. Sauter, A. Sushkov, Nuclear Fusion **41**(11), 1663 (2001). DOI 10.1088/0029-5515/41/11/316. URL `https://doi.org/10.1088/0029-5515/41/11/316`

107. A. Pochelon, T. Goodman, M. Henderson, C. Angioni, R. Behn, S. Coda, F. Hofmann, J.P. Hogge, N. Kirneva, A. Martynov, J.M. Moret, Z. Pietrzyk, F. Porcelli, H. Reimerdes, J. Rommers, E. Rossi, O. Sauter, M. Tran, H. Weisen, S. Alberti, S. Barry, P. Blanchard, P. Bosshard, R. Chavan, B. Duval, Y. Esipchuck, D. Fasel, A. Favre, S. Franke, I. Furno, P. Gorgerat, P.F. Isoz, B. Joye, J. Lister, X. Llobet, J.C. Magnin, P. Mandrin, A. Manini, B. Marlétaz, P. Marmillod, Y. Martin, J.M. Mayor, J. Mlynar, C. Nieswand, P. Paris, A. Perez, R. Pitts, K. Razumova, A. Refke, E. Scavino, A. Sushkov, G. Tonetti, F. Troyon, W.V. Toledo, P. Vyas, Nuclear Fusion **39**(11Y), 1807 (1999). DOI 10.1088/0029-5515/39/11y/321. URL `https://doi.org/10.1088/0029-5515/39/11y/321`

108. R. Holger, MHD stability limits in the TCV tokamak. Ph.D. thesis, Ecole Polytechnique Fédérale de Lausanne (EPFL), Lausanne (2001). DOI 10.5075/epfl-thesis-2399. URL `http://infoscience.epfl.ch/record/32875`

109. M. Bussac, R. Pellat, D. Edery, J. Soule, Physical Review Letters **35**(24), 1638 (1975)

110. A. Martynov, Ideal mhd stability of tokamak plasmas with moderate and low aspect ratio. Ph.D. thesis, Ecole Polytechnique Fédérale de Lausanne (EPFL), Lausanne (2001). DOI 10.5075/epfl-thesis-3218. URL `http://infoscience.epfl.ch/record/33686`

111. F. Porcelli, D. Boucher, M. Rosenbluth, Plasma Physics and Controlled Fusion **38**(12), 2163 (1996)

112. O. Sauter, C. Angioni, D. Boucher, I. Furno, A. Pochelon, F. Porcelli, Theory of Fusion Plasmas, Proc. of the joint Varenna–Lausanne Int. Workshop (Varenna, 1998) ed J W Connor, E Sindoni and J Vaclavik (Bologna: Editrice Compositori) p. 403 (1999)

113. H. Reimerdes, I. Furno, F. Hofmann, A. Martynov, A. Pochelon, O. Sauter, Plasma Physics and Controlled Fusion **48**(11), 1621 (2006). DOI 10.1088/0741-3335/48/11/004. URL `https://doi.org/10.1088/0741-3335/48/11/004`

114. H. Weisen, J.M. Moret, S. Franke, I. Furno, Y. Martin, M. Anton, R. Behn, M. Dutch, B. Duval, F. Hofmann, B. Joye, C. Nieswand, Z. Pietrzyk, W.V. Toledo, Nuclear Fusion **37**(12), 1741 (1997). DOI 10.1088/0029-5515/37/12/i07. URL `https://doi.org/10.1088/0029-5515/37/12/i07`

115. E.A. Lazarus, F.L. Waelbroeck, T.C. Luce, M.E. Austin, K.H. Burrell, J.R. Ferron, A.W. Hyatt, T.H. Osborne, M.S. Chu, D.P. Brennan, P. Gohil, R.J. Groebner, C.L. Hsieh, R.J. Jayakumar, L.L. Lao, J. Lohr, M.A. Makowski, C.C. Petty, P.A. Politzer, R. Prater, T.L. Rhodes, J.T. Scoville, E.J. Strait, A.D. Turnbull, M.R. Wade, G. Wang, H. Reimerdes, C. Zhang, Plasma Physics and Controlled Fusion **48**(8), L65 (2006). DOI 10.1088/0741-3335/48/8/l01. URL `https://doi.org/10.1088/0741-3335/48/8/l01`

116. N.A. Kirneva, K.A. Razumova, A. Pochelon, R. Behn, S. Coda, L. Curchod, B.P. Duval, T.P. Goodman, B. Labit, A.N. Karpushov, M. Rancic, O. Sauter, M.S. and, Plasma Physics and Controlled Fusion **54**(1), 015011 (2012). DOI 10.1088/0741-3335/54/1/015011. URL `https://doi.org/10.1088/0741-3335/54/1/015011`

117. A.H. Glasser, J.M. Greene, J.L. Johnson, The Physics of Fluids **18**(7), 875 (1975). DOI 10.1063/1.861224. URL `https://aip.scitation.org/doi/abs/10.1063/1.861224`

118. H. Lütjens, Magnetohydrodynamic stability of internal kink modes in tokamaks application of an equilibrium code using bicubic finite elements. Ph.D. thesis, Ecole Polytechnique Fédérale de Lausanne (EPFL), Lausanne (1993). DOI 10.5075/epfl-thesis-1105. URL `http://infoscience.epfl.ch/record/31583`

119. C. Atanasiu, G. Günter, K. Lackner, A. Moraru, A. Subbotin, 28th EPS Conf. on Contr. Fusion and Plasma Physics, Funchal, 18-22 June 2001, ECA Vol. 25A (2008) **25A**, 1105, P (2001). URL `http://epsppd.epfl.ch/Madeira/html/pdf/P3.048.pdf`

120. C.V. Atanasiu, S. Günter, K. Lackner, A. Moraru, L.E. Zakharov, A.A. Subbotin, Physics of Plasmas **11**(12), 5580 (2004). DOI 10.1063/1.1806477. URL `https://doi.org/10.1063/1.1806477`

121. L. Bernard, F. Helton, R. Moore, Computer Physics Communications **24**(3), 377 (1981). DOI https://doi.org/10.1016/0010-4655(81)90160-0. URL `https://www.sciencedirect.com/science/article/pii/0010465581901600`

122. A. Glasser, Physics of Plasmas **23**(7), 072505 (2016)

123. M. Austin, A. Marinoni, M. Brookman, J. Degrassie, A. Hyatt, C. Petty, S. Smith, K. Thome, M. Walker, G. McKee, C. Sung, High confinement in negative triangularity discharges in diii-d preprint: 2018 iaea fusion energy conf.(gandhinagar, india, 22–27 october 2018). Tech. rep., IAEA-CN-391/EX/P6-6 (2018)

124. M. Siccinio, W. Biel, M. Cavedon, E. Fable, G. Federici, F. Janky, H. Lux, F. Maviglia, J. Morris, F. Palermo, O. Sauter, F. Subba, H. Zohm, Fusion Engineering and Design **156**, 111603 (2020). DOI https://doi.org/10.1016/j.fusengdes.2020.111603. URL `https://www.sciencedirect.com/science/article/pii/S0920379620301514`

125. Y. Nishimura, F.L. Waelbroeck, L.J. Zheng, Physics of Plasmas **27**(1), 012505 (2020). DOI 10.1063/1.5131157. URL `https://doi.org/10.1063/1.5131157`

126. M. Coleman, S. McIntosh, Fusion Engineering and Design **154**, 111544 (2020). DOI https://doi.org/10.1016/j.fusengdes.2020.111544. URL `https://www.sciencedirect.com/science/article/pii/S0920379620300922`

127. L. Zhou, Y. Liu, M. Siccinio, E. Fable, T. Wu, T. Kurki-Suonio, J. Varje, D. Liu, Plasma Physics and Controlled Fusion **63**(6), 065007 (2021). DOI 10.1088/1361-6587/abf446. URL `https://doi.org/10.1088/1361-6587/abf446`

128. G. Becker, K. Lackner, in *Plasma Physics and Controlled Nuclear Fusion Research*, vol. 2 (International Atomic Energy Agency, 1977), vol. 2, pp. 401–409

129. D. Berger, L. Bernard, R. Gruber, F. Troyon, in *Plasma Physics and Controlled Nuclear Fusion Research*, vol. 2 (International Atomic Energy Agency, 1977), vol. 2, pp. 411–420

130. J. Callen, J. Clarke, R. Dory, J. Holmes, F. Marcus, D. McAlees, J. Moore, D. Nelson, Y.K. Peng, R. Sayer, Plasma Physics and Controlled Nuclear Fusion Research 1976, Volume 2 **2**, 369 (1977)

131. M. Chu, D. Dobrott, G. Guest, F. Helton, T. Jensen, J. Luxon, R. Miller, T. Ohkawa, J. Rawls, T. Wang, Plasma Physics and Controlled Nuclear Fusion Research 1976, Volume 2 **2**, 387 (1977)

132. J. Johnson, M. Chance, J. Greene, R. Grimm, S. Jardin, W. Kerner, J. Manickam, K. Weimer, in *Plasma Physics and Controlled Nuclear Fusion Research*, vol. 2 (International Atomic Energy Agency, 1977), vol. 2, pp. 395–400

133. B. Coppi, W. Sadowski, Proceedings of the finite beta theory workshop. Tech. rep., Department of Energy, Washington, DC (USA). Office of Fusion Energy (1977)

134. J. Wesson, Nuclear Fusion **18**(1), 87 (1978). DOI 10.1088/0029-5515/18/1/010. URL https://doi.org/10.1088/0029-5515/18/1/010

135. A. Todd, J. Manickam, M. Okabayashi, M. Chance, R. Grimm, J. Greene, J. Johnson, Nuclear Fusion **19**(6), 743 (1979). DOI 10.1088/0029-5515/19/6/005. URL https://doi.org/10.1088/0029-5515/19/6/005

136. W. Kerner, P. Gautier, K. Lackner, W. Schneider, R. Gruber, F. Troyon, Nuclear Fusion **21**(11), 1383 (1981)

137. C. Schultz, A. Bondeson, F. Troyon, A. Roy, Nuclear Fusion **30**(11), 2259 (1990). DOI 10.1088/0029-5515/30/11/004. URL https://doi.org/10.1088/0029-5515/30/11/004

138. M. Phillips, A. Todd, M. Hughes, J. Manickam, J. Johnson, R. Parker, Nuclear Fusion **28**(9), 1499 (1988). DOI 10.1088/0029-5515/28/9/002. URL https://doi.org/10.1088/0029-5515/28/9/002

139. F. Hofmann, O. Sauter, H. Reimerdes, I. Furno, A. Pochelon, Phys. Rev. Lett. **81**, 2918 (1998). DOI 10.1103/PhysRevLett.81.2918. URL https://link.aps.org/doi/10.1103/PhysRevLett.81.2918

140. M. Kikuchi, R. Conn, F. Najmabadi, Y. Seki, Fusion Engineering and Design **16**, 253 (1991)

141. *ITER International Thermonuclear Experimental Reactor (Establishment of ITER: Relevant Documents)*. No. 1 in ITER Documentation Series (INTERNATIONAL ATOMIC ENERGY AGENCY, Vienna, 1988). URL https://www.iaea.org/publications/1024/iter-international-thermonuclear-experimental-reactor-establishment-of-iter-relevant-documents

142. G. Rewoldt, W.M. Tang, M.S. Chance, The Physics of Fluids **25**(3), 480 (1982). DOI 10.1063/1.863760. URL https://aip.scitation.org/doi/abs/10.1063/1.863760

143. R. Miller, M. Chu, R. Dominguez, T. Ohkawa, Comments on Plasma Physics and Controlled Fusion **12**(3), 125 (1989)

144. J. Kesner, J.J. Ramos, F.Y. Gang, Journal of Fusion Energy **14**(4), 361 (1995)

145. M. Roberto, R.M.O. Galvão, Brazilian Journal of Physics **24**(3), 693 (1994). URL http://sbfisica.org.br/bjp/download/v24/v24a95

146. R.E. Waltz, R.L. Miller, Physics of Plasmas **6**(11), 4265 (1999). DOI 10.1063/1.873694. URL https://doi.org/10.1063/1.873694

147. J.M. Moret, M. Anton, S. Barry, R. Behn, G. Besson, F. Buhlmann, A. Burri, R. Chavan, M. Corboz, C. Deschenaux, M.J. Dutch, B.P. Duval, D. Fasel, A. Favre, S. Franke, A. Hirt, F. Hofmann, C. Hollenstein, P.F. Isoz, B. Joye, J.B. Lister, X. Llobet, J.C. Magnin, P. Mandrin, B. Marletaz, P. Marmillod, Y. Martin, J.M. Mayor, J. Moravec, C. Nieswand, P.J. Paris, A. Perez, Z.A. Pietrzyk, V. Piffl, R.A. Pitts, A. Pochelon, O. Sauter, W. van Toledo, G. Tonetti, M.Q. Tran, F. Troyon, D.J. Ward, H. Weisen, Plasma Physics and Controlled Fusion **37**(11A), A215 (1995). DOI 10.1088/0741-3335/37/11a/014. URL https://doi.org/10.1088/0741-3335/37/11a/014

148. J. Ren, Y. Liu, Y. Liu, S.Y. Medvedev, Z. Wang, G. Xia, Plasma Physics and Controlled Fusion **58**(11), 115009 (2016). DOI 10.1088/0741-3335/58/11/115009. URL https://doi.org/10.1088/0741-3335/58/11/115009

149. T. Ohkawa, Tokamak configurations with average magnetic well for trapped particles. Tech. rep., General Atomics (1988)

150. R.G. Mills, Tokamak configurations with average magnetic well for trapped particles. Tech. rep., Princeton Plasma Physics Laboratory (1974)

151. D. Meade, in *Plasma Physics and Controlled Nuclear Fusion Research* (International Atomic Energy Agency, 1980), pp. 665–677

152. J.M. Moret, S. Franke, H. Weisen, M. Anton, R. Behn, B.P. Duval, F. Hofmann, B. Joye, Y. Martin, C. Nieswand, Z.A. Pietrzyk, W. van Toledo, Phys. Rev. Lett. **79**, 2057 (1997). DOI 10.1103/PhysRevLett.79.2057. URL https://link.aps.org/doi/10.1103/PhysRevLett.79.2057

153. A. Pochelon, Z.A. Pietrzyk, T.P. Goodman, M. Henderson, H. Reimerdes, M. Tran, R. Behn, S. Coda, M.J. Dutch, B.P. Duval, I. Furno, F. Hofmann, J.P. Hogge, J.B. Lister, X. Llobet, Y. Martin, J.M. Moret, C. Nieswand, J. Rommers, O. Sauter, W. van Toledo, G. Tonetti, H. Weisen, Y.V. Esipchuk, A.A. Martynov, 2nd Europhysics Topical Conf. on RF Heating of Fusion Devices **22A**, 253 (1998)

154. Y. Camenen, A. Pochelon, A. Bottino, S. Coda, F. Ryter, O. Sauter, R. Behn, T.P. Goodman, M.A. Henderson, A. Karpushov, L. Porte, G. Zhuang, Plasma Physics and Controlled Fusion **47**(11), 1971 (2005). DOI 10.1088/0741-3335/47/11/007. URL `https://doi.org/10.1088/0741-3335/47/11/007`

155. Y. Camenen, Étude du transport d'énergie thermique dans les plasmas du tokamak à configuration variable au moyen de chauffage électronique cyclotronique. Ph.D. thesis, Ecole Polytechnique Fédérale de Lausanne (EPFL), Lausanne (2006). DOI 10.5075/epfl-thesis-3618. URL `https://infoscience.epfl.ch/record/87520`

156. R.E. Waltz, G.M. Staebler, W. Dorland, G.W. Hammett, M. Kotschenreuther, J.A. Konings, Physics of Plasmas **4**(7), 2482 (1997). DOI 10.1063/1.872228. URL `https://doi.org/10.1063/1.872228`

157. Y. Camenen, A. Pochelon, R. Behn, A. Bottino, A. Bortolon, S. Coda, A. Karpushov, O. Sauter, G. Zhuang, the TCV team, Nuclear Fusion **47**(7), 510 (2007). DOI 10.1088/0029-5515/47/7/002. URL `https://doi.org/10.1088/0029-5515/47/7/002`

158. A. Marinoni, S. Coda, R. Chavan, G. Pochon, Review of Scientific Instruments **77**(10), 10E929 (2006). DOI 10.1063/1.2222333. URL `https://doi.org/10.1063/1.2222333`

159. M. Fontana, L. Porte, S. Coda, O.S. and, Nuclear Fusion **58**(2), 024002 (2017). DOI 10.1088/1741-4326/aa98f4. URL `https://doi.org/10.1088/1741-4326/aa98f4`

160. M. Fontana, Turbulence studies in TCV using the correlation ece diagnostic. Ph.D. thesis, Ecole Polytechnique Fédérale de Lausanne (EPFL), Lausanne (2018). DOI 10.5075/epfl-thesis-9016. URL `http://infoscience.epfl.ch/record/258091`

161. Z. Huang, S.C. and, Plasma Physics and Controlled Fusion **61**(1), 014021 (2018). DOI 10.1088/1361-6587/aadb59. URL `https://doi.org/10.1088/1361-6587/aadb59`

162. Z. Huang, Experimental study of plasma turbulence in the TCV tokamak. Ph.D. thesis, Ecole Polytechnique Fédérale de Lausanne (EPFL), Lausanne (2017). DOI 10.5075/epfl-thesis-7715. URL `http://infoscience.epfl.ch/record/230348`

163. A. Marinoni, S. Brunner, Y. Camenen, S. Coda, J.P. Graves, X. Lapillonne, A. Pochelon, O. Sauter, L. Villard, Plasma Physics and Controlled Fusion **51**(5), 055016 (2009). DOI 10.1088/0741-3335/51/5/055016. URL `https://doi.org/10.1088/0741-3335/51/5/055016`

164. W. Han, N. Offeddu, T. Golfinopoulos, C. Theiler, C. Tsui, J. Boedo, E. Marmar, the TCV Team, Nuclear Fusion **61**(3), 034003 (2021). DOI 10.1088/1741-4326/abdb95. URL `https://doi.org/10.1088/1741-4326/abdb95`

165. F. Riva, C.K. Tsui, J.A. Boedo, P. Ricci, Physics of Plasmas **27**(1), 012301 (2020). DOI 10.1063/1.5123451. URL `https://doi.org/10.1063/1.5123451`

166. M. Fontana, L. Porte, S. Coda, O. Sauter, S. Brunner, A.C. Jayalekshmi, A. Fasoli, G.M. and, Nuclear Fusion **60**(1), 016006 (2019). DOI 10.1088/1741-4326/ab4d75. URL `https://doi.org/10.1088/1741-4326/ab4d75`

167. S. Coda, S. Brunner, M. Faitsch, M. Fontana, Z. Huang, A. Iantchenko, A. Merle, G. Merlo, A. Pochelon, L. Porte, H. Reimerdes, O. Sauter, Bull. Am. Phys. Soc. **64**, GP10.00097 (2019)

168. M. Kotschenreuther, G. Rewoldt, W. Tang, Computer Physics Communications **88**(2), 128 (1995). DOI https://doi.org/10.1016/0010-4655(95)00035-E. URL `https://www.sciencedirect.com/science/article/pii/001046559500035E`

169. A. Marinoni, Plasma fluctuation studies in the TCV tokamak modeling of shaping effects and advanced diagnostic development. Ph.D. thesis, Ecole Polytechnique Fédérale de Lausanne (EPFL), Lausanne (2009). DOI 10.5075/epfl-thesis-4516. URL `http://infoscience.epfl.ch/record/140631`

170. F. Jenko, W. Dorland, M. Kotschenreuther, B.N. Rogers, Physics of Plasmas **7**(5), 1904 (2000). DOI 10.1063/1.874014. URL `https://doi.org/10.1063/1.874014`

171. G. Merlo, S. Brunner, O. Sauter, Y. Camenen, T. Görler, F. Jenko, A. Marinoni, D. Told, L. Villard, Plasma Physics and Controlled Fusion **57**(5), 054010 (2015). DOI 10.1088/0741-3335/57/5/054010. URL `https://doi.org/10.1088/0741-3335/57/5/054010`

172. G. Merlo, Flux-tube and global grid-based gyrokinetic simulations of plasma microturbulence and comparisons with experimental TCV measurements. Ph.D. thesis, Ecole Polytechnique Fédérale de Lausanne (EPFL), Lausanne (2016). DOI 10.5075/epfl-thesis-7065. URL `http://infoscience.epfl.ch/record/219007`

173. O. Sauter, S. Brunner, D. Kim, G. Merlo, R. Behn, Y. Camenen, S. Coda, B.P. Duval, L. Federspiel, T.P. Goodman, A. Karpushov, A. Merle, T. Team, Physics of Plasmas **21**(5), 055906 (2014). DOI 10.1063/1.4876612. URL `https://doi.org/10.1063/1.4876612`

174. B. Kadomtsev, O. Pogutse, Sov. Phys.—JETP **24**(6), 1172 (1967). URL `http://www.jetp.ac.ru/cgi-bin/e/index/e/24/6/p1172?a=list`

175. C. Zucca, O. Sauter, E. Asp, S. Coda, E. Fable, T.P. Goodman, M.A. Henderson, Plasma Physics and Controlled Fusion **51**(1), 015002 (2008). DOI 10.1088/0741-3335/51/1/015002. URL `https://doi.org/10.1088/0741-3335/51/1/015002`

176. J.P. Graves, Plasma Physics and Controlled Fusion **55**(7), 074009 (2013). DOI 10.1088/0741-3335/55/7/074009. URL `https://doi.org/10.1088/0741-3335/55/7/074009`

177. G. Merlo, Z. Huang, C. Marini, S. Brunner, S. Coda, D. Hatch, D. Jarema, F. Jenko, O. Sauter, L. Villard, Plasma Physics and Controlled Fusion **63**(4), 044001 (2021). DOI 10.1088/1361-6587/abe39d. URL `https://doi.org/10.1088/1361-6587/abe39d`

178. G. Merlo, M. Fontana, S. Coda, D. Hatch, S. Janhunen, L. Porte, F. Jenko, Physics of Plasmas **26**(10), 102302 (2019). DOI 10.1063/1.5115390. URL `https://doi.org/10.1063/1.5115390`

179. M.A. Beer, Gyrofluid models of turbulent transport in tokamaks. Ph.D. thesis, Princeton University (1995). URL `https://catalog.princeton.edu/catalog/944800`

180. A. Marinoni. H-mode-like confinement with L-mode edge in negative triangularity plasmas on DIII-D (2017). Presented at the 3rd Asia Pacific conference on Plasma Physics, Hefei, China

181. S. Saarelma, M.E. Austin, M. Knölker, A. Marinoni, C. Paz-Soldan, L. Schmitz, P.B. Snyder, Plasma Physics and Controlled Fusion (2021). URL `http://iopscience.iop.org/article/10.1088/1361-6587/ac1ea4`

182. J. Candy, E. Belli, R. Bravenec, Journal of Computational Physics **324**, 73 (2016). DOI https://doi.org/10.1016/j.jcp.2016.07.039. URL `https://www.sciencedirect.com/science/article/pii/S0021999116303400`

183. G.M. Staebler, J.E. Kinsey, R.E. Waltz, Physics of Plasmas **14**(5), 055909 (2007). DOI 10.1063/1.2436852. URL `https://doi.org/10.1063/1.2436852`

184. D. Whyte, A. Hubbard, J. Hughes, B. Lipschultz, J. Rice, E. Marmar, M. Greenwald, I. Cziegler, A. Dominguez, T. Golfinopoulos, N. Howard, L. Lin, R. McDermott, M. Porkolab, M. Reinke, J. Terry, N. Tsujii, S. Wolfe, S. Wukitch, Y.L. and, Nuclear Fusion **50**(10), 105005 (2010). DOI 10.1088/0029-5515/50/10/105005. URL `https://doi.org/10.1088/0029-5515/50/10/105005`

185. J.R. Dorris, J.C. Rost, M. Porkolab, Review of Scientific Instruments **80**(2), 023503 (2009). DOI 10.1063/1.3065094. URL `https://doi.org/10.1063/1.3065094`

186. G.R. McKee, R.J. Fonck, M.W. Shafer, I.U. Uzun-Kaymak, Z. Yan, Review of Scientific Instruments **81**(10), 10D741 (2010). DOI 10.1063/1.3495788. URL `https://doi.org/10.1063/1.3495788`

187. C. Sung, W.A. Peebles, C. Wannberg, T.L. Rhodes, X. Nguyen, R. Lantsov, L. Bardóczi, Review of Scientific Instruments **87**(11), 11E123 (2016). DOI 10.1063/1.4961296. URL `https://aip.scitation.org/doi/abs/10.1063/1.4961296`

188. M.A. Van Zeeland, C. Collins, W. Heidbrink, M. Austin, X. Du, V. Duarte, A. Hyatt, G. Kramer, N. Gorelenkov, B. Grierson, D. Lin, A. Marinoni, G. McKee, C. Muscatello, C. Petty, C. Sung, K. Thome, M. Walker, Y. Zhu, Nuclear Fusion **59**(8), 086028 (2019). DOI 10.1088/1741-4326/ab2488. URL `https://doi.org/10.1088/1741-4326/ab2488`

189. M.A. Van Zeeland, G.J. Kramer, M.E. Austin, R.L. Boivin, W.W. Heidbrink, M.A. Makowski, G.R. McKee, R. Nazikian, W.M. Solomon, G. Wang, Phys. Rev. Lett. **97**, 135001 (2006). DOI 10.1103/PhysRevLett.97.135001. URL `https://link.aps.org/doi/10.1103/PhysRevLett.97.135001`

190. N. Gorelenkov, H. Berk, E. Fredrickson, S. Sharapov, JET EFDA Contributors, Physics Letters A **370**(1), 70 (2007). DOI https://doi.org/10.1016/j.physleta.2007.05.113. URL `https://www.sciencedirect.com/science/article/pii/S0375960107007451`

191. A.D. Turnbull, E.J. Strait, W.W. Heidbrink, M.S. Chu, H.H. Duong, J.M. Greene, L.L. Lao, T.S. Taylor, S.J. Thompson, Physics of Fluids B: Plasma Physics **5**(7), 2546 (1993). DOI 10.1063/1.860742. URL `https://doi.org/10.1063/1.860742`

192. Y. Kusama, H. Kimura, T. Ozeki, M. Saigusa, G. Kramer, T. Oikawa, S. Moriyama, M. Nemoto, T. Fujita, K. Tobita, G. Fu, R. Nazikian, C. Cheng, Nuclear Fusion **38**(8), 1215 (1998). DOI 10.1088/0029-5515/38/8/308. URL `https://doi.org/10.1088/0029-5515/38/8/308`

193. C.Z. Cheng, M.S. Chance, The Physics of Fluids **29**(11), 3695 (1986). DOI 10.1063/1.865801. URL `https://aip.scitation.org/doi/abs/10.1063/1.865801`

194. V. Duarte, H. Berk, N. Gorelenkov, W. Heidbrink, G. Kramer, R. Nazikian, D. Pace, M. Podestà, B. Tobias, M.A. Van Zeeland, Nuclear Fusion **57**(5), 054001 (2017). DOI 10.1088/1741-4326/aa6232. URL `https://doi.org/10.1088/1741-4326/aa6232`

195. W. Heidbrink, C. Collins, L. Stagner, Y. Zhu, C. Petty, M.V. Zeeland, Nuclear Fusion **56**(11), 112011 (2016). DOI 10.1088/0029-5515/56/11/112011. URL `https://doi.org/10.1088/0029-5515/56/11/112011`

196. J. Breslau, M. Gorelenkova, F. Poli, J. Sachdev, X. Yuan, U.O. of Science. TRANSP computer software (2018). DOI 10.11578/dc.20180627.4. URL `https://www.osti.gov/biblio/1489900`

197. M. Faitsch, R. Maurizio, A. Gallo, S. Coda, T. Eich, B. Labit, A. Merle, H. Reimerdes, B. Sieglin, C. Theiler, and, Plasma Physics and Controlled Fusion **60**(4), 045010 (2018). DOI 10.1088/1361-6587/aaaef7. URL `https://doi.org/10.1088/1361-6587/aaaef7`

198. R. Maurizio, B. Duval, B. Labit, H. Reimerdes, M. Faitsch, M. Komm, U. Sheikh, C. Theiler, the TCV team and, Nuclear Fusion **61**(2), 024003 (2021). DOI 10.1088/1741-4326/abd147. URL `https://doi.org/10.1088/1741-4326/abd147`

199. A. Marinoni, M. Austin, A. Hyatt, S. Saarelma, F. Scotti, Z. Yan, C. Chrystal, S. Coda, F. Glass, J. Hanson, A. McLean, D. Pace, C. Paz-Soldan, C. Petty, M. Porkolab, L. Schmitz, F. Sciortino, S. Smith, K. Thome, F. Turco, Nuclear Fusion (2021). URL `http://iopscience.iop.org/article/10.1088/1741-4326/ac1f60`

200. S.C. Hsu, M. Artun, S.C. Cowley, Physics of Plasmas **3**(1), 266 (1996). DOI 10.1063/1.871852. URL `https://doi.org/10.1063/1.871852`

201. T. Happel, T. Puetterich, J. Hobirk, H. Zohm, the ASDEX Upgrade Team, Bull. Am. Phys. Soc. **65**, TO10.00009 (2020)